KTH Elektro-
och systemteknik

Electrical Insulating Properties of Poly(Ethylene-*co*-Butyl Acrylate) Filled with Alumina Nanoparticles

NADEJDA JÄVERBERG

Doctoral Thesis
Stockholm, Sweden 2013

TRITA-EE 2013:005
ISSN 1653-5146
ISBN 978-91-7501-647-4

KTH School of Electrical Engineering
SE-100 44 Stockholm
SWEDEN

Akademisk avhandling som med tillstånd av Kungl Tekniska högskolan framlägges till offentlig granskning för avläggande av teknologie doktorsexamen onsdagen den 27 februari 2013 klockan 10.00 i F3, Lindstedtsvägen 26, Kungl Tekniska högskolan, Stockholm.

Tryck: Universitetsservice US AB

Abstract

In this work the electrical insulating properties of the nanocomposite materials based on poly(ethylene-*co*-butyl acrylate) filled with alumina nanoparticles are studied. The dielectric properties chosen for the evaluation are the dielectric permittivity and loss as well as the breakdown strength and the pre-breakdown currents. The reason for choosing these particular properties is partly due to the importance of these for the general electrical applications and partly due to the uncertainties involved for these particular properties of the nanocomposite materials.

The importance of moisture absorption for the dielectric properties is outlined in this work. All measurements were performed in both dry conditions and after conditioning of the materials in humid environment until saturation. The data for moisture absorption was taken from the water absorption study performed at the Department of Fibre and Polymer Technology, KTH.

The dielectric spectroscopy in frequency domain was employed for measuring dielectric permittivity and loss. Havriliak-Negami approximation was used for characterization of the measurement data and at the same time ensuring the fulfillment of the Kramers-Kronig relations. Results from the dielectric spectroscopy study in dry conditions suggest that dielectric spectroscopy can be used for evaluating nanoparticle dispersion in the host matrix, based on correlation between the morphology data obtained from SEM investigation and the scatter in the dielectric loss. The dielectric spectroscopy study performed on the nanocomposites after conditioning in humid environment showed that absorbed moisture has a distinct impact on the dielectric loss. Especially pronounced is its' influence on the frequency behavior, when the dielectric loss peaks are shifted towards higher frequencies with increased moisture content. The nanocomposite materials characterized by higher specific surface area generally exhibit higher dielectric losses. Surface functionalization of the nanoparticles does not seem to have much influence on the dielectric loss in dry conditions. After conditioning in humid environment, however, the surface modification was shown to have a significant impact. Temperature is another significant factor for the frequency behavior of the dielectric loss: it was found that the studied nanocomposites can be characterized by Arrhenius activation.

The breakdown strength and pre-breakdown currents study outlined the influence of moisture as well. The study indicated that surface treatment of the nanoparticles can enhance properties of the nanocomposite materials, namely aminopropyltriethoxy silane was an especially successful choice:

- The highest breakdown strength was determined by the study for NDA6 material formulation in dry conditions.
- After conditioning in humid environment the NDA6 material continued showing the best breakdown strength among the nanocomposite mate-

rials, as well as this value was close to the breakdown strength of the reference unfilled material.

This study confirms the existence of the optimal nanofiller content or rather optimal specific surface area of the dispersed nanoparticles in the host matrix. The latter is supported by the comparison between the nanocomposites based on nanoparticles with two different specific surface areas, which shows that the dielectric properties worsen, i.e. the dielectric losses increase and the influence of absorbed moisture on the breakdown strength becomes more pronounced, for nanomaterials with larger specific surface area. The pre-breakdown currents were found to follow space-charge limited conduction mechanism reasonably well. The following conduction regimes were identified: constant region (likely due to measurement difficulties at low field strengths), Ohm's regime, trap-filled-limit regime and trapfree dielectric regime. The breakdown usually occurred either during the trap-filled-limit regime, when the current increased dramatically for the small change in electric field, or during the trapfree dielectric regime. The threshold values between different conduction regimes seem to correlate well with the oxidation induction times (OIT), which in turn depend on the total specific surface area. The pre-breakdown currents tend to be highest for the materials filled with the untreated nanoparticles. Increased absorbed moisture content causes higher pre-breakdown currents for the nanocomposite materials, while for the reference unfilled material the pre-breakdown currents do not show such tendency. Generally it can be said that the repeatability in the measured data is higher for the nanocomposite materials in comparison to the unfilled host material, as was demonstrated by both dielectric spectroscopy and breakdown studies.

Keywords: nanocomposites, poly(ethylene-*co*-butyl acrylate), EBA, alumina, dielectric permittivity, absorbed water, humidity, temperature, dielectric spectroscopy, breakdown strength, pre-breakdown current

Acknowledgements

First and foremost I would like to thank my supervisor Hans Edin for all the support, help and encouragement during the course of this project. He was always there for me whenever I needed help or encouragement.
My deep thanks go to all the members of the nano-project group: Patricia Nordell, Sohail Nawaz, Henrik Hillborg, Bruska Azhdar and Ulf W. Gedde for providing feedback and sharing valuable knowledge that helped me greatly along the way. I am very grateful to Henrik Hillborg for both the input into explaining how the mysterious world of polymers work and the insight into scientific reasoning as well as laboratory work. I will always remember Henrik's rule of π. My special thanks go to Patricia Nordell for putting up with my endless questions and also for all the fruitful discussions we had both in the lab and during lunch breaks. I would also like to thank Lars Jonsson for the valuable discussions and for proof-reading this thesis with many comments, Venkatesulu Bandapalle for all the hours we spent on data analysis, lab work and writing papers, and the most recent addition to our group - Elena Kubyshkina, who I wish best of luck in her complicated task of modeling nanocomposite materials.
I am very grateful to Nathaniel Taylor, Cecilia Forséen and Valentinas Dubikas for making me feel welcome in the high-voltage research group when I just started with this project, and to Xiaolei Wang, Mohamad Ghaffarian Niasar, Respicius Clemence, Håkan Westerlund and Roya Nikjoo for creating a wonderful and friendly atmosphere to work in. My special thanks go to Nathaniel Taylor for introducing me to the mysterious world of the IDA and all the discussions, sharing ideas and also for posting the latex cheat sheet on my notice board (even though it was done in a very sneaky way in the night) that helped me greatly with writing this thesis. He will always be my role model when it comes to finding ways of finishing things even if it takes sitting and working long time into the night.
Many thanks to Yelena Vardanyan for friendship and patience in discussing statistics and maths, and Tetiana Bogodorova for being a friend, inspiring me to work harder on my project and pointing out new angles of thinking.
Big thanks to all my colleagues from both Electromagnetic Engineering and Power Systems departments for being so friendly and brightening up my day. I must say I really enjoyed being a Ph. D. student here.
I would also like to thank all the members of the reference group in the nano-project - Thomas Liljenberg (ABB) and Clair Pitois (ABB) for helping me to become more goal-oriented and focused in my work; Sven Jansson (Elforsk) for always being kind and supportive; Eva Malmström (KTH), Christian Andersson (Ericsson), Niclas Schönborg (Svenska Kraftnät) and Erik Perzon (Borealis) for providing feedback and guidance.
The project was funded by the Swedish Energy Agency, Elforsk AB, ABB AB, Swedish Railway Company, Ericsson AB (Cables & Interconnect) and Borealis via the ELEKTRA program, grant 36120, and is gratefully acknowledged.
Last but not the least I would like to thank my family for all the encouragement

and support they've given me.

Nadja Jäverberg
Stockholm, February 2013

List of publications:

This thesis is based on the following papers:

I "Dielectric Properties of Alumina-filled poly(ethylene-*co*-butyl acrylate) Nanocomposites", N. Jäverberg, H. Edin, P. Nordell, H. Hillborg, B. Azhdar and U.W. Gedde, 2010 Annual Report Conference on Electrical Insulation and Dielectric Phenomena, West Lafayette, USA, October 2010

II "Influence of Moisture on Dielectric Properties of Alumina-filled poly(ethylene-*co*-butyl acrylate) Nanocomposites", N. Jäverberg and H. Edin, Nordic Insulation Symposium, Tampere, Finland, June, 2011

III "Dielectric Properties of Alumina-filled poly(ethylene-*co*-butyl acrylate) Nanocomposites, part I - dry studies", N. Jäverberg, H. Edin, P. Nordell, S. Nawaz, H. Hillborg, B. Azhdar and U.W. Gedde, IEEE Transactions on Dielectrics and Electrical Insulation Vol. 19, No. 2, 2012, pp. 383 - 390

IV "Dielectric Properties of Alumina-filled poly(ethylene-*co*-butyl acrylate) Nanocomposites, part II - wet studies", N. Jäverberg, H. Edin, P. Nordell, S. Nawaz, H. Hillborg, B. Azhdar and U.W. Gedde, IEEE Transactions on Dielectrics and Electrical Insulation Vol. 19, No. 2, 2012, pp. 391 - 399

V "Dielectric Breakdown Strength of Alumina Filled Poly (ethylene-*co*-butyl acrylate) Nanocomposites", N. Jaeverberg, B. Venkatesulu and H. Edin, IEEE Conference on Electrical Insulation and Dielectric Phenomena, Montreal, Canada, October 2012, pp. 323 - 326

VI "Prebreakdown Current and Breakdown Strength of Alumina-filled Poly(ethylene-*co*-butyl acrylate) Nanocomposites: Part I - Breakdown Strength", N. Jaeverberg, B. Venkatesulu, H. Edin and H. Hillborg, submitted to IEEE Transactions on Dielectrics and Electrical Insulation

VII "Prebreakdown Current and Breakdown Strength of Alumina-filled Poly(ethylene-*co*-butyl acrylate) Nanocomposites: Part II - Prebreakdown Currents", N. Jaeverberg, B. Venkatesulu, H. Edin and H. Hillborg, submitted to IEEE Transactions on Dielectrics and Electrical Insulation

VIII "Influence of Applied Voltage and Temperature on the Current through the Alumina-filled poly(ethylene-*co*-butyl acrylate) Nanocomposites Under Constant Stress", N. Jaeverberg, B. Venkatesulu, and H. Edin, to be submitted to Nordic Insulation Symposium 2013

Nomenclature:

A	area
A_{FN}	field-independent coefficient in the equation for Fowler-Nordheim injection
A_{RD}	Richardson-Dushman constant
α	constant in Havriliak-Negami approximation
B_{FN}	field-independent coefficient in the equation for Fowler-Nordheim injection
β	constant in Havriliak-Negami approximation
β_{PF}	Poole-Frenkel constant
β_S	Schottky field-lowering coefficient
$\widetilde{C}$	complex capacitance
C'	real part of the complex capacitance
C''	imaginary part of the complex capacitance
C_0	geometric capacitance
σ_{DC}	DC conductivity
σ_0	low field conductivity
D	displacement field
d	sample thickness
E	electric field strength
E_{act}	activation energy
E_g	energy gap
e	electron charge
ϵ_0	permittivity of free space
$\widetilde{\epsilon}$	complex permittivity
ϵ'	real part of complex permittivity
ϵ''	imaginary part of complex permittivity
ϵ_r	relative permittivity
$\epsilon''_{r,app}$	apparent dielectric loss factor, which combines contributions from both conduction and the polarization losses
ϵ_∞	permittivity at sufficiently high frequencies where losses are negligible
$\mathcal{F}(x)$	Fourier transform of a function x
f_{diel}	dielectric response function
ϕ	work function of the electrode
I	current
J	current density
J_0	low field current density
j	imaginary unit
k_B	Boltzmann's constant
λ	jump distance
μ	charge mobility
ω	angular frequency
ω_p	angular frequency of a loss peak
P	polarization
T	temperature

t	time
$tan\delta$	loss tangent
τ	variable of integration
U, V	voltage
x	variable of integration
$\widetilde{\chi}$	complex susceptibility
χ'	real part of complex susceptibility
χ''	imaginary part of complex susceptibility
χ_∞	susceptibility at sufficiently high frequencies where losses are negligible
Z	impedance

Abbreviations:

BDS	electric field strength at breakdown
DS	dielectric spectroscopy
A or amino silane	Aminopropyltriethoxy silane
O or octyl silane	Octyltriethoxy silane
EBA	poly(ethylene-*co*-butyl acrylate) with 13 wt% butyl acrylate
ND	NanoDur nanoparticles
NA	NanoAmor nanoparticles
NDU	nanocomposite filled with unmodified NanoDur nanoparticles
NDA	nanocomposite filled with NanoDur nanoparticles surface-treated with aminopropyltriethoxy silane
NDO	nanocomposite filled with NanoDur nanoparticles surface-treated with octyltriethoxy silane
NAU	nanocomposite filled with unmodified NanoAmor nanoparticles
NAA	nanocomposite filled with NanoAmor nanoparticles surface-treated with aminopropyltriethoxy silane
NAO	nanocomposite filled with NanoAmor nanoparticles surface-treated with octyltriethoxy silane
SCLC	space charge limited conduction
TFS	trap free square
TFL	trapfilled limit
TSSA	total specific surface area
OIT	oxidation induction time

Contents

Chapter 1

Introduction

1.1 Background

The concept of the nanodielectrics is comparatively recent [1], [2] even though the nanocomposite materials have been used for many centuries. One of the earliest known nanocomposites was used for making the Lycurgus cup, dating back to 4th century AD [3]. From the perspective of electrical applications nanodielectrics can be seen as the next generation of filled materials after microfilled dielectrics. Microfillers are conventionally used for enhancing mechanical and thermal material properties, which unfortunately quite often leads to impairment of electrical properties, such as decrease in breakdown strength [4], increase in space charge accumulation [5], etc. The ultimate goal with introducing nanostructured dielectrics is a possibility of tailoring the electrical properties to fit the desired application, still keeping the advantage of the enhanced thermal and mechanical properties. Such improvements as suppression of space charge formation [6], increase in breakdown strength [7], [8], improved partial discharge resistance [7], enhanced voltage endurance (increased initiation and propagation times for electrical treeing) [7], etc. were reported for various nanocomposites. One of the major difficulties in production of the nanocomposite materials is achieving good dispersion of the nanoparticles in the polymer matrix. Having such small dimensions ($<$ 100 nm in at least one dimension) nanoparticles tend to agglomerate. The smaller the nanoparticles are - the larger is the specific surface area which means larger interfacial zone between the particles and the host matrix. It is the interfaces that are attributed the changes in the material properties [9], [10], and [11]. There seems to be, however, a percolation limit above which the dielectric properties of a nanocomposite worsen. This maximum nanoparticle loading seems to be different for different nanoparticles and host matrices: between 2 and 5 wt% for various host matrices and fillers as reported in the literature [11], close to 6 wt% as found in this study [3], [12], and [13]. Intuitively, this percolation limit can be explained with the help of the multicore model [14]. The multicore model considers a nanoparticle imbed-

ded into a polymer base matrix, which is represented by a sphere surrounded by three concentric layers: the bonded, bound and loose layers, along with the Gouy - Chapman diffuse layer overlapping the first three layers. If the filler loading is low then these layers do not overlap for the neighboring particles and the particles do not "feel" each other. With the increasing filler content the overlapping between the interfacial layers of neighboring particles will start to occur. So that at some filler content the entire material can be seen as an interfacial zone between the filler particles and the polymer base matrix. If the filler content is too high then the forces between the neighboring particles will become significant, making e.g. the homogenous dispersion of the nanoparticles in the matrix hard to achieve.

It is possible to calculate the specific surface area in ideal case, i.e. in the absence of agglomerates of the particles in the polymer host matrix. Unfortunately, the agglomerates can be present in real life conditions as well as there can be a certain nanoparticle size distribution that will affect the specific surface area. Hence, the effective specific surface area, i.e. the available specific surface area that accounts for the latter, could be a better way of describing the interfacial zone between the nanoparticles and the host polymer matrix. The main disadvantage with this term is the difficulty associated with the estimation of the true effective specific surface area.

1.2 Literature review

Tailoring of nanocomposites' electrical properties has been a goal since it was shown that there exists such a possibility [15], [16], [17]. Opposed to microcomposite materials the electric properties of the nanocomposites, such as the dielectric permittivity, cannot be modeled with ease with the help of effective medium theories [18], such as e.g. Maxwell-Garnett formula [19]. For some cases though it did prove to be successful as reported in [20] and [21], also a numerical model based on Maxwell-Garnett formula was proposed for composites filled with conducting nanoparticles in [22].

A lot of research has been done in order to cover such dielectric properties as dielectric permittivity and loss (dielectric spectroscopy), dc conductivity at low and high electric fields, space charge, dielectric breakdown (AC, DC, impulse), treeing resistance, partial discharge resistance, tracking resistance and flame retardancy [23]. Some of these properties, e.g. treeing lifetime and partial discharge resistance, were shown to improve while the other, e.g. breakdown strength as well as dielectric permittivity and loss, could either increase or decrease depending on the nanocomposite studied. Naturally a proper dispersion of the nanoparticles in the host polymer matrix without any agglomerates is vital for obtaining the enhancement in the electric properties.

The breakdown strength, dielectric permittivity and dielectric loss are very important properties for any material to be used as insulation. The reports on the breakdown strength vary. It has been reported that the results for the AC breakdown strength for nanocomposite materials can be inconclusive [24], [25], [26]. The AC breakdown strength can increase in some cases [27], [23] or it can stay unchanged [23]. The DC breakdown strength has been known to increase for the nanocomposites in comparison to the unfilled polymer matrix [28], [27] or stay the same as for the base unfilled material [29], [23]. The trend for the decreasing breakdown strength with increasing filler content is common for both the AC and the DC breakdown strength studies [28], [29]. It can be claimed that there exists optimal filler content for the maximal breakdown strength of a nanocomposite material [16], [30]. Moisture seems to have a degrading effect on the breakdown strength as reported in [30], [31], [29], [32]; it also seems to cause the increase in conduction currents [32]. The influence of temperature on the breakdown strength is complicated, depending on the studied material [33]. E.g. for LDPE, the closest to the EBA materials studied in this work, the breakdown strength above room temperature decreases with increasing temperature [33].

The dielectric permittivity was shown to increase or decrease with addition of nanoparticles [24], [28], [34], [35], [29], [25], [26], [27], [23], [36] likely depending on the mechanism dominating for a specific nanocomposite formulation: either steered by filler permittivity, which can cause an increase in the dielectric constant, or the restriction of the polymer chains' movements in the interface zone between the nanoparticles and the host matrix, which could explain a decrease in the dielectric constant [35]. The behavior of a dielectric loss of a nanocomposite is hard to predict. It seems that it can either stay very close to the base material [34], [29] or there can be a small change [24], [25], [27]. It has also been found that the low frequency dispersion can be suppressed for the nanocomposites in comparison to the unfilled base matrix [36]. As to the influence of moisture, it has been found to have a significant effect on the electric properties even at small amounts of absorbed moisture [37], [32], [29]. Absorbed moisture often leads to increased dielectric permittivity of a material [37]. A concept of filler aspect ratio, i.e. the proportion between the width and the height of a filler particle, was suggested as an explanation for this influence [32]. This explanation is based on a water shell model [38]. So that the filler with the higher aspect ratio is characterized by a lower breakdown strength due to easier formation of percolation paths between the neighboring water shells, which also means higher conduction currents. The influence of temperature on the dielectric loss follows Arrhenius activation for both unfilled polymers and nanocomposites [39], [40].

1.3 Aim

The aim of this work was to evaluate the insulating properties of the nanocomposite materials based on poly(ethylene-*co*-butyl acrylate) filled with alumina nanopowder. The following properties were studied:

- the dielectric permittivity and loss
- the breakdown strength and the pre-breakdown current

These properties were studied as a function of particle functionalization, specific surface area (which includes such parameters as particle size and filler content), humidity and temperature. Dielectric permittivity was measured with the help of dielectric spectroscopy. Measurements were performed both on thoroughly dried materials and after conditioning in humid environment; in the dry case temperature was varied as well.

The breakdown strength was evaluated by a progressive electrical stress test based on a modified standard measurement method for evaluating breakdown strength of films and tapes [41]. The pre-breakdown current was measured with a current amplifier up to breakdown during the breakdown study. Materials were also tested by a constant stress test at different temperature levels.

The importance of moisture absorption for the dielectric properties of nanocomposite materials is explored.

1.4 Thesis outline

This thesis is based on Papers I - VIII. The introduction to this work is given in Chapters 1-3.
Chapter 2 describes the materials used in this work and provides a summarized explanation of nanocomposite manufacturing performed at the Department of Fiber and Polymer Technology, KTH [42].
Chapter 3 contains a short theoretical summary.
Chapter 4 contains a description of used experimental evaluation methods.
Chapter 5 presents all experimental results from this work and discussion.
Chapter 6 summarizes the publications that lay ground for this thesis, namely Papers I-VIII.
General conclusions and suggestions for possible future work are described in Chapter 7.

1.5 Author's contributions

The author has done the majority of work for Papers I-VII. The description of the nanocomposite manufacturing is based on the work performed at the Department

of Fiber and Polymer Technology, KTH [42]. Docent Henrik Hillborg was involved in discussion and analysis of the experimental data obtained in Papers III, IV, VI and VII. The measurements and data analysis presented in Papers V - VII were performed in collaboration with postdoctoral researcher Venkatesulu Bandapalle. Experimental work described in Paper VIII was made by postdoctoral researcher Venkatesulu Bandapalle.

This work was supervised by Docent Hans Edin (Department of Electromagnetic Engineering, KTH).

Chapter 2

Material description

Polyethylene is one of the most common insulation materials, e.g. it is often used for cable manufacturing. This served as basis for choosing it as the base material in this study. Polar butyl acrylate was added to the polyethylene in order to improve nanoparticle dispersion in the polymer.

2.1 Materials

As host matrix poly(ethylene-*co*-butyl acrylate) polymer was used. It contained 13 wt% butyl acrylate groups and was supplied by Borealis, Stenungsund, Sweden. The density of this polymer was 924 kg/m^3 and the melt flow index [1] was 1.1 g/10 min.

Two types of alumina nanopowder were used:

- NanoDur (ND) nanoparticles were supplied by Nanophase Inc., USA. These nanoparticles were larger in size - in average 45 nm in diameter, spherical in shape, consisting of 70% δ-phase and 30 % γ-phase. The specific surface area was 36 m^2/g, see Fig. 2.1(a).
- NanoAmor (NA) nanoparticles were supplied by Nanostructured & Amorphous Materials Inc., USA. These nanoparticles were smaller - in average 25 nm in diameter of irregular shape consisting of γ-phase. The specific surface area was 180 m^2/g, see Fig. 2.1(b).

In order to stabilize the material further the antioxidant Irganox 1010 (a hindered phenolic antioxidant) supplied by Ciba Specialty Chemicals, Germany, was used.
Two types of silane were used for nanoparticle functionalization:

[1] according to ISO 1133 (190 $^\circ C$, 2.16 kg weight)

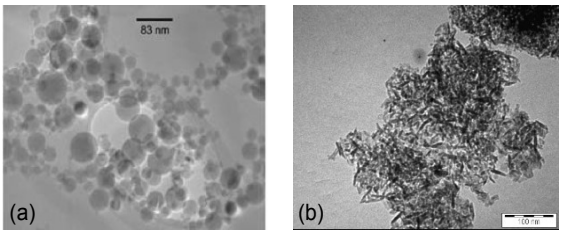

Figure 2.1: Micrographs obtained at the Department of Fiber and Polymer Technology [42]: (a) NanoDur and (b) NanoAmor nanoparticles.

- Aminopropyltriethoxy silane, supplied by Sigma-Aldrich.
- Octyltriethoxy silane, supplied by Fluka.

All materials and chemicals were used as received.

2.2 Nanocomposite manufacturing

Here only a short summary of the manufacturing process is presented, see [42] for a thorough description.

Prior to mixing, the nanoparticles were dried in vacuum at 190 $°C$ for 24 h. This stage was followed by functionalization of the nanoparticles surfaces. The nanoparticles were split into three groups: first one was used as received for the uncoated case, second one was surface-treated with amino silane and the third one was surface-modified with octyl silane. All three groups were dried once more in vacuum at 110 $°C$ for 24 h.

The host polymer was ground and sieved to the maximum size of 500 nm. This powder was mixed then with slurry, consisting of 90 wt% nanoparticles, 0.2 wt% of antioxidant and the rest was isopropanol. A three-dimensional ultramixer Turbula Shaker Mixer Type T2F, WAG, Switzerland, was used to blend the mixture for 3h at room temperature. The obtained mixture was dried at 70 $°C$ for 2 h, followed by another mixing in the ultramixer at 50 $°C$ for 2 h and finally dried at 50 $°C$ for 24 h at 1 kPa pressure. The dried mixture was then extruded twice to obtain tape-shaped films of approximately 1 mm thickness.

The reference unfilled material, i.e. EBA with antioxidant, was also produced.

2.3 Nanocomposite post-processing

In order to obtain thinner samples the received tapes were compressed in vacuum to the thickness of approximately 140 μm using the TP 400 polymer press from Fontijne Grotnes, see Fig. 2.2 for the conditions for temperature and pressure used during the compression molding. Finally the thickness was measured with a 227-221 Mitutoyo digital micrometer with the measurement force set to 0.5 N and accuracy of 4 μm.

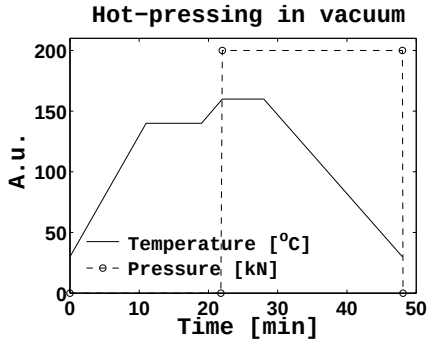

Figure 2.2: Temperature (solid line) and pressure (dashed line with circle markers) used for post processing nanocomposite tapes in the polymer press

2.4 Experimental matrix and sample conditioning

Altogether 18 material variations were manufactured for this work; see Fig. 2.3 for the entire experimental matrix evaluated in this work. The coding for each material consists of three letters followed by a number:

- The number shows the filler content of the nanoparticles in the polymer host material. It can be 2, 6 or 12 wt%.
- The first two letters denote the nanoparticle type used for this specific material: either "ND" (NanoDur) or "NA" (NanoAmor) nanoparticles
- The third letter stands for the type of particle functionalization: either "A" for amino silane, "O" for octyl silane or "U" for untreated nanoparticles

An example for the material coding can be seen in Fig. 2.3.

All the materials evaluated in this work were either thoroughly dried or conditioned in a humid environment at different levels of humidity. The latter was attempted in order to see the influence of moisture absorption on dielectric properties. The drying was performed in vacuum in two stages - first at 50 $°C$ for 48

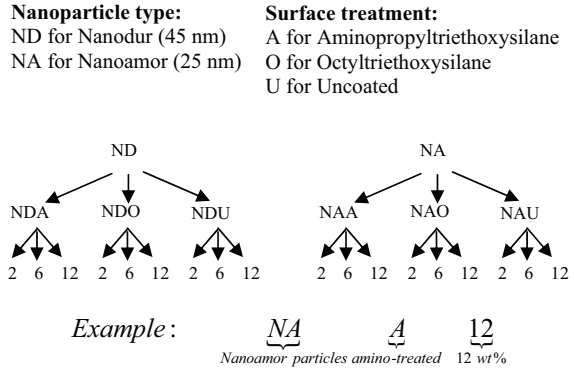

Figure 2.3: Coding of the materials

h, followed by 60 $^{\circ}C$ for 24 h, based on water absorption study performed in [42]. After the drying stage the samples were either stored in a desiccator filled with the orange silica gel from Merck KGaA at room temperature, or further conditioned in a humid environment. This conditioning was also performed in a desiccator where the humidity level was set up by using a salt solution. Humidity was measured continuously by a Testo 608-H2 hygrometer to ensure stable environment. Three different humidity levels were used in this work:

- 24 %RH, obtained by using a salt solution of potassium acetate which was supplied by Merck Chemicals
- 54 %RH, obtained by using a salt solution of sodium bromide which was supplied by KEBO Lab
- 86 %RH, obtained by using a salt solution of zinc sulphate heptahydrate which was supplied by VWR International

A water absorption study of the nanocomposite materials along with the reference unfilled material at the levels of humidity comparable to the ones used in this work, namely 20, 50 and 90 %RH, was performed at the Department of Fiber and Polymer technology, KTH [42]. Based on the mentioned water absorption study the data for moisture content was used for estimation of moisture content absorbed by the materials in this work. Firstly, the minimal times needed to reach saturation were recalculated in order to account for the difference in sample thickness according to Eq.(2.1). Secondly, the samples were conditioned for longer times than the calculated ones to ensure the saturation. Considering that the spread in the measured data for the "wet" materials was smaller than the corresponding spread in the data for the "dry" materials, see Papers III, IV, VI and VII, it is feasible that the materials did reach saturation.

$$t_{new} = t_{old}(\frac{d_{new}}{d_{old}})^2 \tag{2.1}$$

Here t stands for time to saturation with moisture, d is the sample thickness, "old" stands for the data obtained in the water absorption study and "new" points at the values used in this work. The extracted data on time to saturation was summarized in Tables 4.5 and 4.6 in the earlier licentiate work [3], and is given here in order to make this thesis more complete, see Tables 2.1 and 2.2.

Table 2.1: Times to saturation and the amount of water uptake for the nanocomposite materials along with the reference unfilled material as extracted from [3]. Here ^{a} stands for data obtained after conditioning for 900 h, when the moisture content still did not reach saturation.

Material	Thickness [mm]	Time to saturation [h]			Water uptake [%]		
		20 %RH	50 %RH	90 %RH	20 %RH	50 %RH	90 %RH
NAU2	1.6	625	100	100	0.08	0.08	0.12
NAU6	1.5	625	400	900	0.17	0.22	0.45
NAU12	1.4	625	400	900	0.30	0.45	0.90^a
NAA2	0.9	900	100	100	0.08	0.04	0.13
NAA6	0.8	900	225	600	0.14	0.12	0.30
NAA12	0.8	900	225	900	0.19	0.23	0.75^a
NAO2	0.8	400	100	100	0.03	0.05	0.08
NAO6	0.9	400	100	625	0.10	0.13	0.25
NAO12	0.8	400	25	900	0.16	0.25	0.43^a
NDU2	1.5	400	50	100	0.04	0.03	0.07
NDU6	1.5	400	50	100	0.07	0.05	0.08
NDU12	1.4	400	100	400	0.05	0.07	0.14
NDA2	0.8	400	25	100	0.05	0.03	0.04
NDA6	0.8	400	400	100	0.06	0.06	0.06
NDA12	0.8	400	400	400	0.05	0.08	0.12
NDO2	0.8	400	100	100	0.03	0.05	0.03
NDO6	0.8	400	100	100	0.05	0.06	0.06
NDO12	0.8	400	400	144	0.05	0.08	0.09
REF	1.4	400	24	24	0.03	0.04	0.06

2.5 Nanocomposites: study of morphology

In this section a summary of a morphology study performed in [42] is given, as morphology is expected to have a significant effect on the electrical data. Generally it can be said that the dispersion of the nanoparticles in the host polymer was

Table 2.2: Time required for saturation of nanocomposite materials at different humidity levels of ambient environment, corrected for the thickness effect

Materials	Humidity [%RH]	Thickness [μm]	Time [h]	Materials	Humidity [%RH]	Thickness [μm]	Time [h]
	20	145	5.1		20	149	3.9
NAU2	50	127	0.6	NDU2	50	146	0.5
	90	138	0.7		90	150	1.0
	20	152	6.4		20	138	3.4
NAU6	50	125	2.8	NDU6	50	133	0.4
	90	140	7.8		90	150	1.0
	20	151	7.3		20	133	3.6
NAU12	50	147	4.4	NDU12	50	146	1.1
	90	135	8.4		90	146	4.4
	20	144	23		20	135	11.4
NAA2	50	137	2.3	NDA2	50	148	0.9
	90	152	2.9		90	147	3.4
	20	140	27.6		20	135	11.4
NAA6	50	139	6.8	NDA6	50	147	13.5
	90	139	18.1		90	142	3.2
	20	152	32.5		20	151	14.3
NAA12	50	140	6.9	NDA12	50	146	13.3
	90	153	32.9		90	148	13.7
	20	136	11.6		20	148	13.7
NAO2	50	147	3.4	NDO2	50	140	3.1
	90	130	2.6		90	136	2.9
	20	146	10.5		20	140	12.3
NAO6	50	138	2.4	NDO6	50	134	2.8
	90	141	15.3		90	139	3.0
	20	142	12.6		20	142	12.6
NAO12	50	146	0.8	NDO12	50	144	13.0
	90	142	28.4		90	146	4.8
	20	159	5.2				
REF	50	147	0.3				
	90	143	0.3				

Table 2.3: Average number of particles in small agglomerates as determined by SEM on a total area of approximately 2 mm^2 and surface coverage of nanoparticles by silane based on weight loss data by thermogravimetry (extracted from [42])

Nanoparticle type	Average number of particles in small agglomerates			Surface coverage [μmol silane/m^2]
	2 wt%	6 wt%	12 wt%	
NDU	3.4	2.6	3.5	0
NDO	2.1	1.5	2.6	0.7
NDA	2.5	2.4	4.1	2.2
NAU	15	21	18	0
NAO	3.2	3.1	3.1	2.3
NAA	3.7	13	8.8	4.2

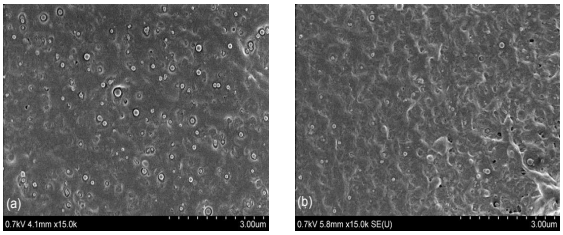

Figure 2.4: SEM micrographs of ND-filled nanocomposites with (a) octyl- and (b) amino-treated nanoparticles (taken at the Department of Fiber and Polymer Technology [42]).

better for the bigger nanoparticles, i.e. ND. Highest filler content, i.e. 12 wt%, had the most agglomerates in comparison to 2 and 6 wt% materials. As expected, surface functionalization had a positive influence on the dispersion; in that respect the nanoparticles treated with octyl silane were easier to disperse in the host polymer than the amino-treated ones. The dispersion was found to be satisfactory for all ND-filled nanocomposites. The smaller nanoparticles, i.e. NA, were harder to disperse. The tendency for the influence of the filler content and the surface treatment on dispersion was the same as for the ND-filled materials. The summary of the dispersion results can be found in Table 2.3. A few SEM photos are shown in Fig. 2.5 and 2.5, see [42] for more SEM photos and the thorough description of the nanoparticle dispersion in the host polymer.

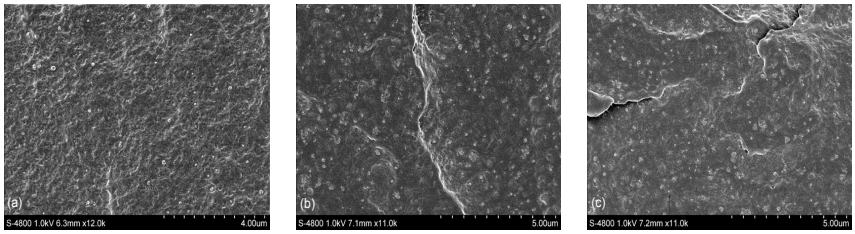

Figure 2.5: SEM micrographs of NA-filled nanocomposites with filler content of (a) 2 wt%, (b) 6 wt% and (c) 12 wt% of amino-treated nanoparticles (taken at the Department of Fiber and Polymer Technology [42]).

Chapter 3

Evaluation methods

3.1 Dielectric properties

A lot of work has been done in the literature on the theory of electrostatics of the dielectrics, e.g. [43], [44], [45], hence only a short summary will be presented in this chapter. An ideal *dielectric* material can be characterized by an absence of free charges; only bound charges exist with the entire material as a whole being neutral. If a dielectric is placed in an electric field the *bound charges*, i.e. the charges that are bound to the atoms and molecules in the material, will rearrange themselves in the field, creating a local electric field. This process is known as *polarization*. There are a number of possible polarization mechanisms, such as:

- *Electronic*, i.e. when placed in an external electric field the positively charged nucleus is displaced in one direction and the negatively charged electron cloud deforms in another direction in an atom, creating a dipole.
- *Ionic*, i.e. when a material consisting of positive and negative ions is placed in an external electric field the ions will be displaced in accordance with the direction of the applied field, creating local dipole moments.
- *Dipolar*, i.e. if a material containing permanent dipoles is placed in an external electric field, then these permanent dipoles will reorient themselves so as to align themselves according to the direction of the applied field, creating net polarization.
- *Interfacial*, i.e. if a material consists of different phases, that can be described with different permittivities and conductivities, is placed in an external electric field charges can accumulate at the interfaces between these phases resulting in a net polarization.
- *Polarization due to hopping charges*, i.e. polarization that can arise due to hopping of the localized charges (e.g. electrons or holes) from one site to a neighboring site in the medium.

In other words polarization takes place under the influence of the applied electric field. A well-known constitutive relation in electromagnetism binds together the electric field **E**, displacement field **D** and the polarization **P**, see Eq.(3.1).

$$\mathbf{D} = \epsilon_0 \mathbf{E} + \mathbf{P} \tag{3.1}$$

If a dielectric material in question is isotropic and linear then this equation can be simplified even further, see Eq.(3.2).

$$\mathbf{D} = \epsilon_0 \mathbf{E} + \mathbf{P} = [\mathbf{P} = \epsilon_0 \widetilde{\chi} \mathbf{E}] = \epsilon_0 \mathbf{E} + \epsilon_0 \widetilde{\chi} \mathbf{E} = \widetilde{\epsilon} \mathbf{E} \tag{3.2}$$

Here $\widetilde{\chi}$ is the complex susceptibility and $\widetilde{\epsilon}$ is the complex permittivity. The electric susceptibility is directly connected to the dielectric response function $f_{diel}(t)$ through Eq.(3.3).

$$\widetilde{\chi}(\omega) = \chi'(\omega) - j\chi''(\omega) = \int_0^\infty f_{diel}(t) \exp^{-j\omega t} \, \mathrm{d}t = \mathcal{F}(f_{diel}(t)) \tag{3.3}$$

$$\begin{aligned} \mathcal{F}(f_{diel}(t)) &= \int_0^\infty f_{diel}(t) \exp^{-j\omega t} \, \mathrm{d}t \\ &= \int_0^\infty f_{diel}(t) \cos \omega t \mathrm{d}t - j \int_0^\infty f_{diel}(t) \sin \omega t \mathrm{d}t = \chi' - j\chi'' \end{aligned} \tag{3.4}$$

Following the calculation in Eq.(3.4) it can be seen that the real part of $\widetilde{\chi}$ is the cosine transform and the imaginary part of $\widetilde{\chi}$ is the sine transform of the dielectric response function. This shows that it should be possible to determine one of the parts if the other one is known. Equations known as Kramers-Kronig relations, discussed e.g. in [37], show this connection, see Eq.(3.5).

$$\begin{aligned} \chi'(\omega) &= \frac{2}{\pi} \int_0^\infty \frac{x\chi''(x)}{x^2 - \omega^2} \mathrm{d}x \\ \chi''(\omega) &= -\frac{2\omega}{\pi} \int_0^\infty \frac{\chi'(x)}{x^2 - \omega^2} \mathrm{d}x \end{aligned} \tag{3.5}$$

Checking whether the Kramers-Kronig relations are satisfied is one of the possible ways of justifying the obtained experimental data. Sometimes in order to avoid complicated mathematical operations one can use an approximation model that was already shown to comply with the Kramers-Kronig relations. Commonly used approximations are for example: Debye response, which is common for such polar dielectric liquids as water and methanol; for solids such common approximations of the dielectric response function are Curie-von Schweidler and Havriliak-Negami, e.g. [37]. There exist quite many other approximations, but in this work it was found that the Havriliak-Negami approximation, see Eq.(3.6), fitted the experimental data very well.

$$\widetilde{\epsilon}(j\omega) = \epsilon_\infty + \frac{\epsilon_0 - \epsilon_\infty}{(1 + (j\frac{\omega}{\omega_p})^{1-\alpha})^{1-\beta}} \tag{3.6}$$

The dielectric response function answers for the slow polarization of the dielectric material, which can be illustrated by Eq.(3.7).

$$\mathbf{P}(t) = \underbrace{\epsilon_0 \chi_\infty \mathbf{E}}_{\text{Fast polarization}} + \underbrace{\epsilon_0 \int_0^t f_{diel}(\tau)\mathbf{E}(t-\tau)\mathrm{d}\tau}_{\text{Slow polarization}} \tag{3.7}$$

3.2 Dielectric spectroscopy

The method behind dielectric spectroscopy is based on measuring the current through a sample when a known voltage is applied to the sample. It is common to calculate then the impedance and consequently the permittivity of the sample. This measurement can be performed in both time and frequency domain. The main advantages of the frequency domain measurements are, firstly, the possibility to reduce the measurement noise by averaging the result measured over several cycles of the same frequency. Secondly, studying permittivity as a function of frequency allows elucidating possible physical processes that can be seen as loss peaks in the frequency domain.

Starting from one of the Maxwell's equations, namely the Ampere's law (see Eq.(3.8)), and remembering Eq.(3.2), it is possible to write down the expression for the total current density through a dielectric in time domain, see Eq.(3.9)). The latter expression can also be rewritten using phasor notations, as can be seen in Eq.(3.10)), so that the total current density through a dielectric medium can be represented with the three terms: first one answering for the DC conduction, second one representing the dielectric losses caused by the movement of the dipoles in the applied electric field and the third one being the pure displacement term.

$$\mathbf{J}(t) = \mathbf{J}_{transport} + \frac{\partial \mathbf{D}}{\partial t} \tag{3.8}$$

$$\mathbf{J}(t) = \sigma_{DC}\mathbf{E}(t) + \frac{\partial}{\partial t}(\widetilde{\epsilon}\mathbf{E}(t)) \tag{3.9}$$

$$\begin{aligned} J(\omega) &= \sigma_{DC}E(\omega) + j\omega(\overbrace{\underbrace{\epsilon'}_{\substack{\text{dielectric}\\\text{constant}}} - j \underbrace{\epsilon''}_{\substack{\text{dielectric}\\\text{loss}}}}^{\widetilde{\epsilon}})E(\omega) \\ &= \underbrace{\sigma_{DC}E(\omega)}_{\text{DC conduction}} + \underbrace{\omega\epsilon''E(\omega)}_{\text{Polarization loss}} + \underbrace{j\omega\epsilon'E(\omega)}_{\text{Pure displacement term}} \\ &= [\widetilde{\epsilon} = \epsilon_0(\epsilon'_r - j\epsilon''_r)] = (\sigma_{DC} + \omega\epsilon_0\epsilon''_r + j\omega\epsilon_0\epsilon'_r)E(\omega) \end{aligned} \tag{3.10}$$

When performing a measurement both terms contributing to the losses, namely the conduction and the polarization losses, will be measured simultaneously. The latter is the reason for introducing the *apparent dielectric loss factor*, which combines contributions from both types of losses, see Eq.(3.11)).

$$\epsilon''_{r,app} = \epsilon''_r + \frac{\sigma_{DC}}{\omega\epsilon_0} \tag{3.11}$$

The sample impedance Z can be calculated once the voltage U across and the current I through the sample are known, see Eq.(3.12)). By presenting the sample as a lossy capacitor with the capacitance $\widetilde{C} = C' - jC'' = C_0(\epsilon'_r - j\epsilon''_r)$ and knowing the geometry, it is possible to calculate the complex permittivity, see Eq.(3.13)). Here C_0 is known as the *geometric capacitance*, i.e. the capacitance of a capacitor with exactly same geometry filled with vacuum instead of a dielectric medium. This approximation holds under following conditions: firstly, the contact between the material and the electrodes must be good, e.g. no air pockets or foreign substances; secondly, the geometry has to allow calculating the geometric capacitance with good accuracy, i.e. preferably a flat object for the parallel-plate capacitor which is easy to work with; thirdly, the edge effects in the electric field have to be insignificant, which can be handled by introducing a guard electrode to ensure homogenous field between the high potential and ground electrodes.

$$Z(\omega) = \frac{U(\omega)}{I(\omega)} = \frac{1}{j\omega\widetilde{C}} \tag{3.12}$$

$$\widetilde{\epsilon}_r = \epsilon'_r - j\epsilon''_r \approx \frac{\widetilde{C}}{C_0} \tag{3.13}$$

Error sources can have a significant influence on the measurements and calculations of the dielectric permittivity. The most obvious factors that can influence the dielectric permittivity are

- Electric field strength; if the electric field strength is low then the current through the material could be too low to be measured correctly.

- Frequency of the applied electric field. The polarization mechanisms are directly connected to the frequency of the applied electric field. For instance a dipole in an electric field will always try to align itself according to the direction of the electric field. If the frequency with which the direction of the electric field alternates is very low then the dipole will have the time needed for the alignment and also the time for staying still in the new position. But if the frequency is really high then the dipole will not have the time to turn all the way the electric field and will only vibrate very close to one position. The loss peak represents the frequency when the dipole has the time to change its direction with 180 °, but does not have any resting time in this new position; which means that it reorients itself in the field all the time generating maximal polarization losses.

- Temperature. Temperature has a noticeable influence on the dielectric permittivity of the polymeric materials; this can be characterized by *Arrhenius activation*, see e.g. [37]. Arrhenius activation follows Eq.(3.14)) and implies that the dielectric permittivity measured at low frequency will be pushed towards higher frequencies. This allows obtaining information at lower frequency than it would have been possible to measure within a reasonable time at room temperature.

$$\omega_p(T_1) = \omega_p(T_2) \exp^{-\frac{E_{act}}{k_B}(\frac{1}{T_2}-\frac{1}{T_1})} \tag{3.14}$$

- Imperfection in the sample shape or in the contact between the sample and the electrodes, both of which affect capacitance and consequently dielectric permittivity calculations.

Another quantity that can be readily measured is the *loss tangent*, see Eq.(3.15)). The main advantage with using the loss tangent is its formal independence on the sample geometry, which means higher accuracy in the measured data than, for instance, for the corresponding dielectric loss factor. The disadvantage with using the loss tangent is its rather complicated relation to the dielectric loss and consequently to the dielectric response function, which describes the behavior of a dielectric in applied electric field.

$$\tan\delta = \frac{\epsilon''_{app}}{\epsilon'} = \frac{\epsilon''_r + \frac{\sigma_{DC}}{\omega\epsilon_0}}{\epsilon'_r} \approx \frac{C''}{C'} \tag{3.15}$$

3.3 Conduction current and breakdown in solids

As stated in the previous section on dielectric spectroscopy, part of the measured current through a dielectric medium, however small, will always be due to conduction, see Eq.(3.10)). There are several known mechanisms that can explain conduction in a dielectric, see e.g. [46], [47], [48]. Generally they can be divided

according to the strength of the applied electric field, i.e. low and high field conduction. When talking about conduction in general, one can talk about the kind of charges that can cause conduction, e.g. electrons (electronic conduction) - here band conduction and hopping conduction mechanisms are often discussed; and ions (ionic conduction) - where intrinsic (i.e. conduction due to dissociation of molecules inside the medium) and extrinsic (i.e. conduction due to impurities) can be discussed. At low fields Ohmic conduction is often observed, even though measurement can be challenging due to very low currents. At high fields the processes become more complicated due to possible bulk (e.g. Poole-Frenkel mechanism) and electrode (e.g. Schottky emission and Fowler-Nordheim tunneling injection) effects, see e.g. [48], [46]. Finally, when the field strength exceeds a critical level, a complete breakdown will follow. Another important factor that influences both conduction in an insulator and breakdown is space charge. The former reflects in space charge limited conduction (SCLC) theory [47].

Here a short summary of the above mentioned mechanisms will be given based on [46], [47], [48].

Ohmic conduction follows Ohm's law which states that the current is directly proportional to the voltage applied to the sample, which in consequence is related to the electric field strength. This law is empiric and was found to explain conduction in many cases.

Poole-Frenkel effect is one of the possible bulk effects, where extra charges are emitted from the traps in the bulk of the insulator due to high field strengths. This process is thermally activated and depends on the strength of the applied electric field, see Eq.(3.16)) for the governing equation.

$$|J| = \sigma_0 |E| \exp^{\beta_{PF} \frac{\sqrt{|E|}}{2k_B T}} \tag{3.16}$$

Where E is electric field strength, k_B is the Boltzmann's constant, T - temperature, σ_0 - low field conductivity, β_{PF} - Poole-Frenkel constant.

Hopping conduction is a thermally activated movement of an electron between adjacent localized states in the bulk of the material. This movement could be either a thermal excitation over a potential barrier, tunneling through it or a combination of both [48]. See Eq.(3.17)) for the equation describing this mechanism.

$$|J| = |J_0| \sinh \frac{e|E|\lambda}{2k_B T} \tag{3.17}$$

Where e is electronic charge, λ - jump distance, J_0 - low field current density.

Schottky emission is a thermionic emission from a metal electrode into a conduction band of a dielectric with consideration given to the mirror charges [46], see Eq.(3.18)).

$$|J| = A_{RD}T^2 \exp^{-\frac{\phi}{k_B T}} \exp \beta_S \frac{\sqrt{|E|}}{k_B T} \tag{3.18}$$

Where A_{RD} is the Richardson-Dushman constant, T is temperature, E - electric field strength, ϕ - work function of the electrode, k_B - Boltzmann's constant, β_S - Schottky field-lowering coefficient.

Fowler-Nordheim injection is the tunneling of electrons through the contact barrier between the metal electrode and the insulator under the influence of high electric field, see Eq.(3.19)).

$$|J| = A_{FN}|E|^2 \exp^{-\frac{B_{FN}}{|E|}} \tag{3.19}$$

Where A_{FN} and B_{FN} are field-independent coefficients.

Space charge limited conduction (SCLC):

Space charge: the charge accumulated at the interfaces in the case of the interfacial polarization is an example of space charge. Space charge can be defined as a localized uncompensated charge of one polarity in a material. Possible reasons for the buildup of space charge can be interfacial polarization, charge injection from the electrodes and also *traps*. Traps can be defined as localized states that appear due to chemical or structural defects that are allowed in the band gap. A *band gap*, as defined by the energy band theory, is an energy range where electron states cannot exist [49]. The band gap can be seen as the minimum energy required to ionize a material in solid state [50], see Fig. 3.1 for a rough illustration of a band structure. The width of a band gap determines how the material behaves in applied electric field. Conductors are characterized by a small band gap < 0.2 eV, for semiconductors the band gap is in the range of 0.2 - 2 eV and for insulators the band gap > 2 eV [48].

The space charge limited conduction theory includes both bulk (e.g. influence of traps in the dielectric) and electrode (i.e. charge injection from the electrodes) effects [46], see Fig. 3.2 for the typical J-E plot. Typically at low fields Ohmic conduction takes place. At higher fields the presence of traps and the associated energy levels will influence as well. So that at a certain threshold the conduction will change from Ohmic to another mode, depending on the presence of traps and their energy, i.e. either to a trap-free square (TFS) law behavior (E^2) if the traps are absent or in the case of deep traps, or Trap-Filled-Limit (TFL) mode ($E^n, n > 2$) if the traps are shallow, as described in [47]. The equation for the TFS law is shown in Eq.(3.20)); here ϵ is the permittivity, μ is the charge mobility, V is

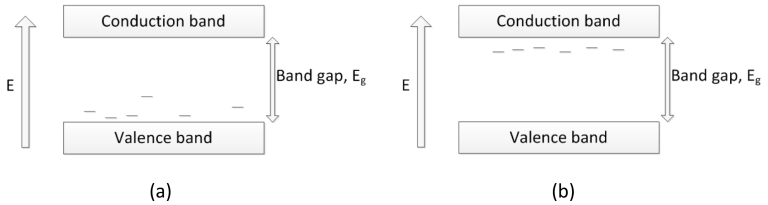

Figure 3.1: An illustration of an energy band structure with a few allowed localized states (traps) in the band gap: (a) deep traps and (b) shallow traps

the applied voltage across the sample (parallel-plate geometry is assumed) and d is the sample thickness. Here it is important to note the dependence of the current density through the sample on the thickness of the sample, which allows a validity check of the SCLC model.

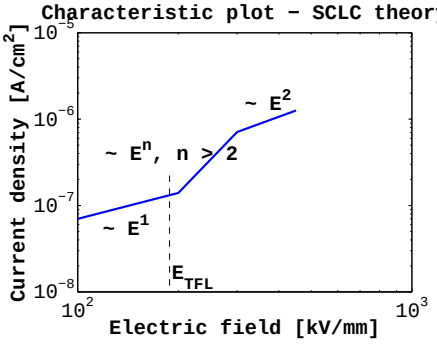

Figure 3.2: A typical plot according to SCLC theory

$$|J| = \frac{9}{8}\frac{\epsilon\mu V^2}{d^3} \tag{3.20}$$

A TFL mode is characterized with a fast increase in current density with a moderately small increase in the electric field, which is thought to be caused by detrapping of the charges that are considered to be trapped for the field strengths below the threshold value E_{TFL} [47]. If there are several sets of traps present then there can be several stages with modes following TFL and trap-free square law, i.e. Ohmic conduction is followed by either TFL or TFS regime and then the mode changes in the sequence of either TFL - TFS - TFL - TFS or TFS - TFL - TFS and so on, depending on the trap distribution and whether the material is capable of sustaining the electric field. At some point the sample will break down.

Breakdown is a complex phenomenon which results in a physical puncture of a ma-

terial in such a way that locally the insulator turns into a conductor. Breakdown can be a result of different mechanisms, such as for example intrinsic or thermal breakdown, or it can be caused by different mechanisms working together, such as electromechanical or electrochemical breakdown. A breakdown can also be caused by erosion due to partial discharge activity and consequent electrical treeing. Here a short description for common types of breakdown based on [48], [46], [51] is given:

Intrinsic breakdown is reached when electrons in the valence band gain enough energy to cross the forbidden gap and get excited into the conduction band. The field strengths of the intrinsic breakdown are very high and are therefore very hard to measure experimentally.

Thermal breakdown is caused by heat generation due to conduction and polarization losses. Thermal breakdown is likely in the case when the material fails during the TFL conduction mode due to sharp increase in current [48].

Electromechanical breakdown can occur when both electric and mechanical stresses work together. The electrostatic attraction force between the electrodes is the origin of the mechanical stress.

Electrochemical breakdown is caused by chemical changes that can occur in an insulating material, such as e.g. oxidation (in the presence of air) or hydrolysis (i.e. breakage of polymeric bonds due to the presence of water).

Erosion due to partial discharge activity is caused by the partial discharge activity that erodes the material starting from a cavity inside the insulating material due to the difference in electric stresses in the bulk material and in the cavity. Commonly the electric stress in a cavity is higher than in the bulk material due to the difference in the permittivities. Erosion due to partial discharges can cause electrical treeing, which during electrical tree propagation pushes the electric potential towards the opposite electrode (due to carbonization of the channels) and consequently increases the electric stress on the healthy insulator.

Edge breakdown has to be mentioned here as a complicating factor in experimental measurements. It is commonly lower than the true breakdown strength of the solid and is therefore misleading. The edge breakdown occurs near the edge of the electrode in a weaker medium than the tested insulation (e.g. air), due to field enhancement as a consequence of different permittivities of the tested insulator and the weaker medium.

Chapter 4

Experimental evaluation methods

4.1 Dielectric spectroscopy: measurement instruments and conditions

Instruments IDA200 and IDAX300 were used for the dielectric spectroscopy study. The main difference between the two is that the former is a standalone unit with a built-in computer, while the latter needs a computer for control. Both are capable of measuring the similar frequency range: 0.1 mHz up to 1 kHz for the IDA200 and 0.1 mHz up to 10 kHz for the IDAX300 [52]. Both are capable of generating up to 200 V_{peak} internally with a possibility of connecting a separate voltage amplifier to increase the sample voltage up to 30 kV. In this work, however, only the internal voltage generation was used. The voltage level was chosen to be 200 V_{peak}, which means that the electric field was approximately 1.4 kV/mm for a sample thickness of 140 μm. Measurement inaccuracy depends on the capacitance of the sample and the chosen frequency ranged, see Fig. 4.1.

In order to extend the frequency range for the experimental data for some of the materials the HP 4284A precision LCR meter was used. The LCR meter is capable of generating voltages of maximum 20 V_{peak} for the frequency range between 20 Hz and 1 MHz.

The experimental work on characterization of the nanocomposite materials with the help of the dielectric spectroscopy is summarized in the Papers I - IV. A thorough description of the measurement cell and the experimental setup can be found there. The materials used in this study were conditioned according to the description in Chapter 2: either thoroughly dried (dry study) or conditioned in a humid environment until saturation in a desiccator at different humidity levels, namely 24, 54 and 86 %RH (wet study). Three samples per material were tested in the dry study. Directly after the dry testing each sample was placed in a desiccator designated for conditioning samples in a humid environment. Only one sample per material was tested in a wet study. The order in which the dry samples were tested was random, but for the humid testing all the samples that were tested first in dry

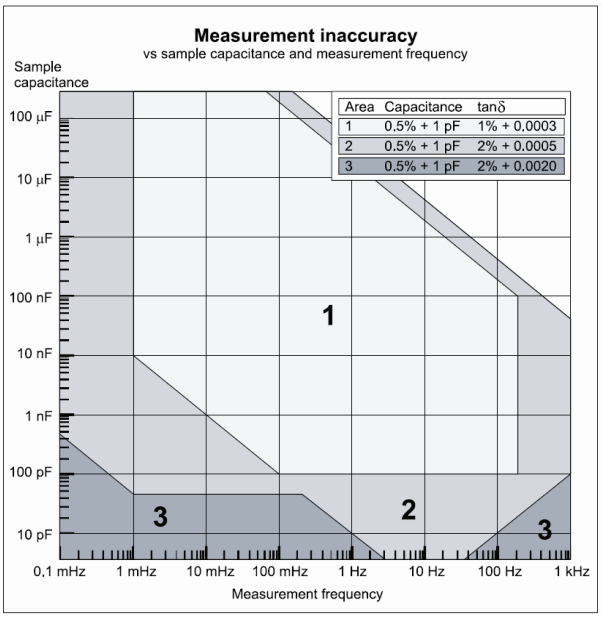

Figure 4.1: Measurement inaccuracy for the IDA200 and IDAX300 [52]

conditions for each specific material were conditioned at 24 %RH, the second ones - in 54 %RH and the third ones - in 86 %RH.

4.2 Dielectric spectroscopy: possible error sources

A rather thorough description of the spread in the experimental data from the dry study and the possible error sources were presented in [3]. Roughly the measurement error can be seen as a combination of the inaccuracy in the magnitude and the inaccuracy in frequency, see Fig. 4.2. The possible error sources include:

1. Instrument inaccuracy, an obvious error source that can influence the inaccuracies in both the magnitude and in the frequency, see Fig. 4.1 for the instrumental inaccuracy.

2. Absorbed moisture has a strong influence on the measurement results. According to the wet study the experimental data curves are displaced towards higher frequencies with higher moisture content. This implies that the absorbed moisture has a strong impact on the inaccuracy in frequency. There can also be some influence on the inaccuracy in the measured magnitude, but not as obvious. For the dry materials all the measurements were performed using synthetic dry air to ensure stable environment during each measurement.

For the 24 %RH the measurement was performed inside a vacuum oven with a salt solution for stabilizing the humidity level, while for the higher humidity levels a climate chamber was used.

3. Temperature is a rather obvious error source due to the well-known Arrhenius activation phenomenon, which shifts the experimental data curves towards higher frequencies for increasing temperatures. This behavior was confirmed for the materials in the dry study, so that it can be claimed that the temperature has a strong impact on the inaccuracy in frequency. The temperature was controlled with a Eurotherm controller to ensure isothermal environment.

4. Pressure on the sample during the measurement can also influence the result. The effect of this factor was minimized in this work by using a spring-loaded measurement cell and allowing each sample to relax for one hour prior to measurement.

5. Possible agglomerates have a pronounced influence on the experimental data as shown in [3]. This factor seems to influence the inaccuracies in both the magnitude and in the frequency. This allows using dielectric spectroscopy as an alternative assessment method of the nanoparticle dispersion in the base polymer matrix.

6. Sample thickness has a strong impact on the magnitude of the dielectric permittivity as the latter is calculated from the experimentally measured capacitance, $\tan\delta$ and sample thickness. The calculation is performed using Eq. 3.13, knowing that C_0 is a geometrical capacitance of a parallel-plate capacitor due to the choice of the measurement cell, i.e. $C_0 = \frac{\epsilon_0 A}{d}$, where A is the measurement electrode area and d is the sample thickness. Hence, the inaccuracy in the sample thickness is directly reflected in the inaccuracy in the magnitude of the dielectric permittivity and the dielectric loss. This was the main reason for presenting the $\tan\delta$ data in the licentiate thesis. Also the differences in the dielectric constant with respect to frequency are rather small, which allowed analyzing $\tan\delta$ data in almost the same way as the dielectric loss. The permittivity is closer, however, to the physical processes in a material. Hence, the data for the calculated dielectric permittivity will be presented here, see [3] for the measured $\tan\delta$ data.

Here the importance of the guard gap, see Fig.2 in Paper II for the illustration of the guard gap (i.e. the distance between the ground and guard electrodes), for the measurements of the dielectric permittivity and loss has to be mentioned as well. Namely, during the initial stage of the experimental work a measurement cell with epoxy in the guard gap was used. When measuring in the room temperature the resulting dielectric constant seemed to be very reasonable, but at higher temperatures the dielectric constant dropped below one. After recalculating the results and analyzing the experimental setup it was found that the epoxy in the guard gap started to conduct at temperatures above room temperature. So that part of

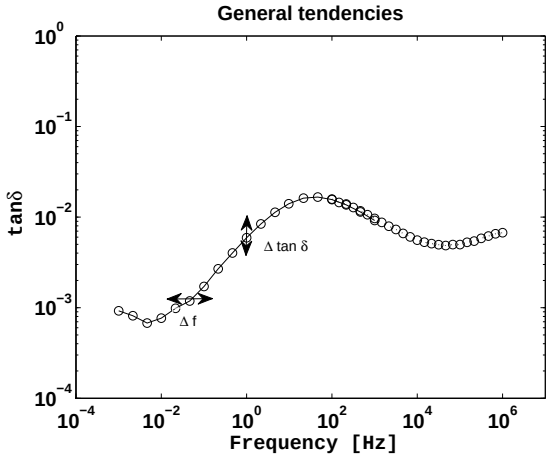

Figure 4.2: Illustration of error sources (the shown errors are enlarged and out of proportion)

the current from the measurement electrode was flowing through the gap to the guard and then was redirected straight to the ground potential. The reason for this was a small difference in potential (∼100 mV) between the measurement electrode and the guard. This meant that lower current was measured and consequently the calculated dielectric constant reduced. In the new measurement cell (the one used in the dielectric spectroscopy study) air was used as the dielectric in the guard gap.

4.3 Breakdown strength and pre-breakdown currents: measurement instruments and conditions

This study was summarized in Papers VI - VIII. Part of this study (Papers VI - VII) was a progressive stress testing performed at room temperature and the other part (Paper VIII) - constant stress testing at temperatures above room temperature.

Progressive stress testing

The instrument setup used for measuring the breakdown strength and the pre-breakdown currents is shown in Fig. 4.3 and was presented in Paper VI. It includes:

- a personal computer (all the controlling programs were written in Matlab) for controlling the function generator and the data recording from the oscilloscope,
- Hewlett-Packard 33120A function generator for generating an amplitude-modified sinusoidal signal as the input to the high voltage amplifier. The

frequency of the sinusoidal was chosen to be 70 Hz in order to minimize the possible interference at 50 Hz; the amplitude of the signal was ramped from zero to 10 V_{peak}, see Fig. 5 in Paper VI for the illustration of a typical signal,

- High voltage amplifier TREK 30/30 for amplifying the signal up to a maximum of 30 kV,
- DC doubler circuit with a high voltage divider that rectifies the output voltage from the TREK and doubles the magnitude, see Fig. 6 in Paper VI for the illustration of a typical applied voltage,
- Metal test chamber with the sample under test immersed in oil, partially for shielding (the chamber is earthed) and partially for evening out the electric field (the dielectric constant for the oil is very close to that of the tested material, which helps avoiding strengthening of the electric fields at the electrode edge),
- Protection circuit for redirecting the current to earth in case of a breakdown,
- Keithley 427 Current amplifier for measuring pre-breakdown currents,
- TDS3052 Tektronix oscilloscope for measuring and recording both applied voltage and the pre-breakdown current.

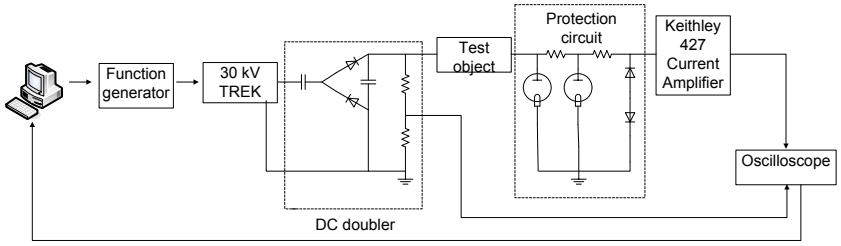

Figure 4.3: Experimental setup for measuring the breakdown strength and pre-breakdown currents in the progressive stress testing (taken from Paper VI).

The oscilloscope readings were obtained in snaps of 4 s with a time step of 400 ms for 50 s. The data was transferred to a computer over an Ethernet connection. The acquisition time varied between 1 and 3 s, the times for starting acquisition were based on the acquisition time of the previous time snap. This leads to either gaps in the data of approximately 1 s or overlaps.

The materials were tested with the help a progressive stress test with the applied voltage ramped up to 60 kV at the rate of 1.2 kV/s. The electrodes used in this study had a diameter of 6 mm with 1 mm edge radius and were made of

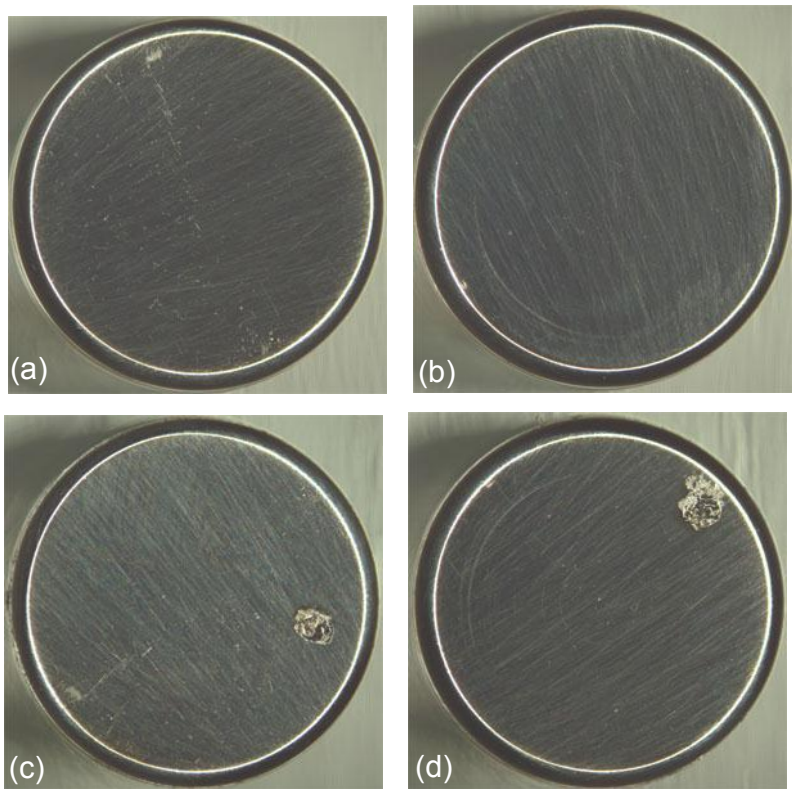

Figure 4.4: A pair of electrodes prior to breakdown strength testing - (a) and (b), and after the test - (c) and (d). The ground electrode is shown in (a) and (c), while the high voltage electrode is shown in (b) and (d).

stainless steel. Each electrode was imaged under a stereo microscope both prior to the experiment and directly after so as to evaluate the influence of existing defects on the results, see Fig.4.4. No correlation was found between the positioning of the shallow defects on the electrode surface and the placing of the actual breakdown. The electrodes with deeper cuts and defects were repolished to ensure that the electrode surface had minimal influence on the experimental results. All used electrodes were repolished and washed carefully in isopropanol after each breakdown.

The materials were conditioned in the same way as for the dielectric spectroscopy study - dry case (the samples were thoroughly dried in vacuum for 48 h at 50 $^{\circ}C$ followed by 24 h at 60 $^{\circ}C$) and wet case (only the humidity level of 86 %RH was used in order to create a reasonably wet environment).

Constant stress testing

This study was described in Paper VIII. For the constant stress testing the instrument setup was modified as shown in Fig. 4.5, namely the DC doubler was removed due to lower voltages needed for the testing. Otherwise the same instruments, measurement cell and electrodes were used. The test voltage was ramped at the speed of 490 V/s up to chosen measurement voltage of either 15 or 22.5 kV_{DC}. The data acquisition and experimental sequence employed were the same as for the progressive stress test. The measurement was performed either until breakdown or up to maximum of 10 minutes. The materials were thoroughly dried prior to testing.

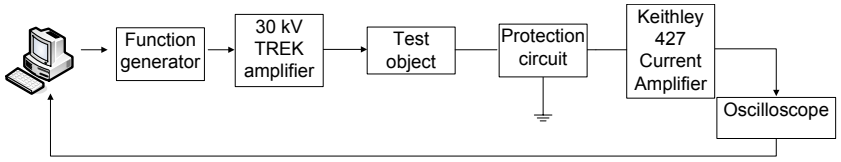

Figure 4.5: Experimental setup for measuring the breakdown strength and pre-breakdown currents in the constant stress testing (taken from Paper VIII).

4.4 Breakdown strength and pre-breakdown currents: possible error sources

A number of possible error sources were identified and minimized during the assembly of the experimental setup. The following sources were addressed:

- Cross-talk between the cables
- Capacitive coupling between the sample and the surroundings
- Ground loop

Other error sources that are harder to influence were:

- Instrument inaccuracy for all of the instruments used, namely the function generator (±1 % [53], which is 0.1 V for a reading of 10 V), the high voltage amplifier (±0.1 % [54], i.e. ±30 V at 30 kV), the current amplifier (±2 % [55], i.e. ±2 nA at 0.1 muA) and the oscilloscope (see Eq.(4.1) [56], which gives ±2.2 kV error for a 60 kV measurement value).

$$\pm(0.02 \cdot reading + 0.05 \cdot div) \tag{4.1}$$

- Absorbed moisture plays an important role in the measurement precision. It can be easily illustrated by the spread in the measured pre-breakdown currents - for the dry materials the spread is larger than for the wet ones. This can be explained primarily by the drying process as the hard bound water in a material is very hard to remove and is subject to both drying time and temperature. Both of these factors were adopted from the water absorption study performed in [42]. Both the time needed for the drying and the temperature were optimized so as to keep experimental times manageable and to avoid material degradation during drying. Other influencing factors connected to the moisture absorption that define the spread in the experimental data are:

  - Times needed for environment stabilization in a desiccator after it has been opened. In order to reduce the influence of this factor two desiccators were employed - one for long-term storage and the other one for sample storage for the samples to be tested on the day of the experimental work. The silica gel used in this study had a color indicator, which allowed easy monitoring. The silica gel was replenished and/or additionally dried on regular basis when needed. A further improvement that can be suggested but was not implemented in this study is to use desiccators capable of sample storage under vacuum conditions.
  - Times between taking the samples out of the desiccator and until the start of the experiment. In order to minimize the consequences of this difficulty all the samples were treated in the same way: a 5 minute rule was enforced during the testing, i.e. the time between taking the sample out of the desiccator and until the experiment start was timed with a stopwatch.

  The materials were tested in a randomized order as an extra safety check. Based on this we believe that the precautions taken for minimization of the influence of the absorbed moisture on the experimental data were satisfactory since no correlation was found between the magnitude of a pre-breakdown current or breakdown strength and the order in which the samples were tested.

- Temperature is an important factor determining both the breakdown strength and the pre-breakdown current. For the part of the study described in Papers VI and VII all the measurements were performed in room temperature with very small variations in temperature; the other part of the study, however, was performed at higher temperatures and is described in Paper VIII. For study performed at temperatures above the room temperature the oil in the test chamber along with the setup and the electrodes were conditioned at the desired temperature level for several hours in order to ensure the isothermal conditions. Temperature was checked with a Fluke sensor on regular basis. We found that the time to breakdown reduced and the currents through the tested samples increased with increasing temperature.

- Possible agglomerates seem to have very small impact on the measurement results for the dry materials, as can be seen in Fig. 4.6(a). It has to be mentioned that the two materials with worst agglomerates, namely NAU6 and NAA6 (see Table 4.1), can be characterized by reasonably high breakdown strength; also the results for these two do not seem to differ from the values obtained for the other materials. This points towards an important observation that none of the agglomerates in the studied materials were severe enough to weaken the material significantly. The results for the wet study are presented in Fig. 4.6(b). Here it can be said that the breakdown strength reduces with increasing agglomeration, NDA6 being the only exception. We believe that the reduction in the breakdown strength is related primarily to the water uptake, which increases with increasing level of agglomeration. It can be argued that the water uptake is higher for the materials with agglomerations present as water gets absorbed and drawn to the agglomerated nanoparticles. So that it tries to envelope each particle individually, penetrating inside the agglomerate and creating large areas with higher conductivity regions. As for the NDA6 material, the nanoparticles are surface-modified with the amino-silane, which has a reactive NH_2 group. This group could act as a charge trapper, which would explain lower pre-breakdown currents and higher breakdown field strengths.

- Sample thickness plays a very important role for determining breakdown field strength E_{BD} due to small thicknesses of the samples ($\sim$140 μm), as the micrometer used in this study is only capable of 4 μm accuracy. This introduces an error of approximately 3 % (for 140 μm thickness) in the thickness measurement and consequently affects the accuracy of E_{BD}.

- Edge breakdown is an issue if there is a difference in the dielectric permittivity between the tested material and the medium used for testing. If the medium has lower permittivity than the material then the value of the obtained breakdown field strength is usually lower than the true breakdown field strength for the sample. In this study a Nytro 10 XN transformer oil was used in order to reduce the risk of partial discharges, also its permittivity is very close to the permittivity of the tested materials (as determined by the dielectric spectroscopy study). An important finding was that no correlation was found between the breakdown field strength and whether the breakdown occurred close to center of the electrodes or close to the edge. This fact allows claiming that the influence of edge breakdown on the measured breakdown field strength was minimal.

All of the above mentioned error sources are important for each individual measurement. Performing several measurements helps to reduce the measurement error. In this work Weibull statistics was used for determining breakdown strength in the progressive stress test, consequently the error in the breakdown strength value was

Table 4.1: Breakdown strength. Here ^{a} denotes that the total surface area of approximately 2 mm^2 was examined in the SEM study [57] and for the material marked with ^{b} the data is based on only 3 samples as only 3 out of 10 tested samples failed

Materials	BDS_{dry} [kV/mm]	BDS_{wet} [kV/mm]	Average number of particles in small agglomerates^a	Water uptake [%]
REF	375	368	N/A	0.06
NDU6	362	247	2.6	0.08
NDA6	444^b	364	2.4	0.06
NDO6	378	287	1.5	0.06
NAU6	415	227	21.0	0.45
NAA6	422	243	13.0	0.30
NAO6	413	248	3.1	0.25

accessed with the help of known formulas for Weibull distribution, see Eq. (4) in Paper VI and Fig.4.6.

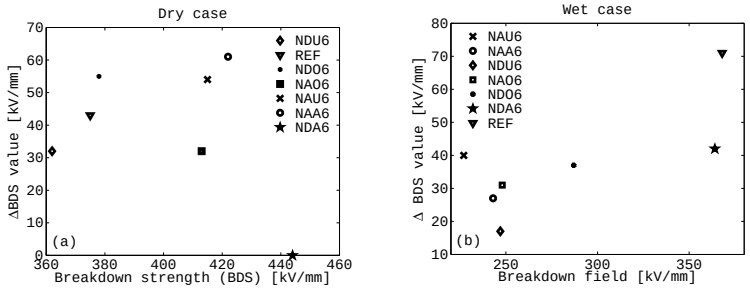

Figure 4.6: The spread in the breakdown field strength (based on Weibull statistics) measured in the progressive stress test versus the breakdown strength for the materials in (a) dry and (b) wet conditions. For the dry conditions the ΔBDS value for the NDA6 material cannot be calculated as only 3 out of 10 tested samples failed.

Chapter 5

Experimental results and discussion

5.1 Dielectric spectroscopy

As was mentioned earlier, the results from the dielectric spectroscopy study will be presented here in the terms of a dielectric permittivity, see Appendix A and B. The tendencies in the data are, however, the same as for the $\tan\delta$. In Paper I the dielectric permittivity was fitted with Havriliak-Negami approximation in order to make sure that the Kramers-Kronig relations were fulfilled and also to justify the experimental data. In the Papers III and IV the behavior of $\tan\delta$ with respect to frequency was analyzed as a function of particle size, filler content, nanoparticle surface modification type, temperature and level of humidity used for material conditioning. The results for the dielectric permittivity can be summarized as follows:

1. Particle size: in the dry case the magnitude of the dielectric constant for the smaller particle size (i.e. NA) was approximately the same as for the larger nanoparticles (i.e. ND) in the case of the untreated nanoparticles; while the magnitude of the dielectric loss was generally higher with the only exception in the case of the materials filled with 2 wt% of uncoated nanoparticles, see Fig. 5.1. This trend is even more pronounced for the dry materials filled with surface-modified nanoparticles and it holds for all the tested temperatures. For the samples conditioned in a humid environment the trend is the same for the dielectric loss.

2. Filler content: for the materials with higher filler content the magnitude of the dielectric loss over entire frequency range is generally higher for both dry and wet cases, see Appendix A and B. This trend is more pronounced for the materials filled with the smaller nanoparticles.

3. Nanoparticle surface modification type: functionalization of the nanoparticles prior to dispersion in the polymer matrix has almost no impact of the dielectric loss with respect to frequency for the dry nanocomposite materials, see Fig. 5.1. But for the wet case on the other hand it plays an important role: the loss peaks for the materials filled with different surface-modified nanoparticles have different characteristic frequencies, which can be related to the number of the OH groups available on the nanoparticles surfaces, see Fig. 5.1. The nanoparticles surface-modified with the amino-silane can be characterized by the highest degree of surface coverage for both ND and NA particles, see Table 2.3. The surface modification can be seen as a partial replacement of the hydroxyl groups with a silane so that the material filled with the amino-treated nanoparticles had the lowest concentration of the hydroxyl groups. Hence the loss peaks for the materials with amino-silanized nanoparticles are placed towards the lower frequencies, followed by the loss peaks corresponding to the materials filled with octyl-silanized nanoparticles and finally the loss peaks for the materials filled with uncoated nanoparticles can be characterized by the highest frequencies. Also the materials filled with octyl-treated nanoparticles exhibit characteristic broad loss peaks which could be explained by two loss peaks being close to each other in frequency: one of which could be caused by water molecules reacting with the OH groups that are left on the surface of the nanoparticles and the other loss peak could be due to the interaction of the water molecules with the octyl-silane.

4. Temperature: the materials studied in this work can be characterized by the Arrhenius activation mechanism as was described in Paper III. The activation energies for all the tested materials are presented in Table 5.1. Also it was determined that the thermal activation differs depending on the frequency range: Arrhenius activation takes place at lower frequencies and something else occurs at higher frequencies. The latter concerns differences with rather small magnitudes, which can look exaggeratingly large in a log-log scale.

5. Humidity: As described above in the 3rd paragraph: Nanoparticle surface modification type, the absorbed moisture plays a significant role for the dielectric loss depending on the type of silane used for surface-modification of the nanoparticles, see Fig. 5.1 and Fig. B.1 (d, e, f) and B.2 (d, e, f) in Appendix B.

    - Concerning the magnitude of $\tan\delta$, it was found that there is a strong correlation between the magnitude of $\tan\delta$ and the filler content (Paper IV), see Table 5.2. The data is summarized only for the materials filled with untreated nanoparticles in order to avoid the influence of the surface modification of the nanoparticles' surfaces. The obtained proportions are quite close to the expected ones, the small deviations are likely due to the measurement inaccuracy of $\tan\delta$.

Table 5.1: Arrhenius activation energies for the tested materials (extracted from Paper III).

Material	Activation energy [eV]	Material	Activation energy [eV]
NDU2	0.93	NAU2	0.94
NDU6	0.80	NAU6	0.87
NDU12	0.82	NAU12	0.93
NDA2	0.77	NAA2	1.00
NDA6	0.85	NAA6	0.96
NDA12	0.95	NAA12	1.16
NDO2	0.73	NAO2	0.72
NDO6	0.81	NAO6	0.67
NDO12	0.78	NAO12	1.37
REF	0.98		

- Concerning frequency dependence we found that the level of humidity used for conditioning of the materials has a significant influence on the frequency dependence of the dielectric loss as can be seen in Fig. 5.1 and Fig. B.1 (d, e, f) and B.2 (d, e, f) in Appendix B. The loss peaks for the same filler content and surface modification exhibit a behavior similar to Arrhenius activation, i.e. the loss peaks are shifted towards higher frequencies for the higher humidity level used for material conditioning. The loss peak magnitude, however, remains largely unchanged for the same filler content and surface modification, with the exception for the materials filled with the octyl surface-treated nanoparticles, where it seems that two loss peaks exist close to each other in frequency. It could be argued that this Arrhenius-like dielectric loss behavior occurs due to a higher mobility of water molecules at the outer borders of the water shells that form around the nanoparticles with increasing moisture absorption. Consequently, this also allows considering that the low frequency dispersion behavior for the nanocomposite materials is actually a part of a loss peak due to hard bound water.

- It has to be noted that the Arrhenius-like shift in dielectric loss towards higher frequencies with increased moisture absorption does not hold for the reference unfilled material, as only the magnitude of the dielectric loss seems to change with increasing moisture absorption, see Fig. B.3 (b) in Appendix B. Hence, addition of the nanoparticles to the polymer matrix should be responsible for any changes in frequency dependence with increased content of absorbed moisture.

Table 5.2: Correlation between the maximum magnitudes of $\tan\delta$ and the filler content

Material	Humidity [wt%]	Measured $\tan\delta$	Theoretically expected proportion (1:3:6)
	24	3.3 : 8.4 : 17.9	3 : 9 : 18
NDU	54	2.7 : 6.9 : 17.2	2.5 : 7.5 : 15
	86	2.3 : 6.5 : 17.1	2 : 6 : 12
	24	8.1 : 25.3 : 57.3	8 : 24 : 48
NAU	54	7.9 : 24.4 : 49.8	8 : 24 : 48
	86	6 : 19.7 : 45.3	6 : 18 : 36

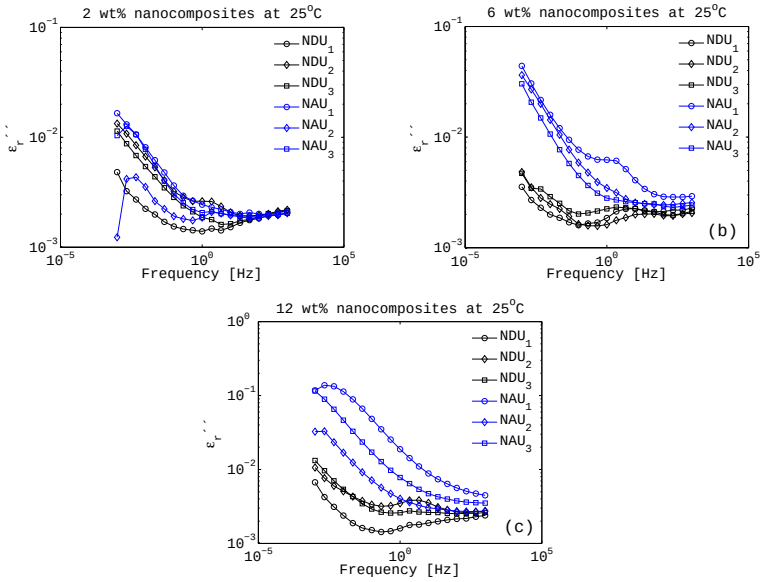

Figure 5.1: Influence of the particle size on the dielectric loss as a function of frequency for the dry materials filled with (a) 2 wt%, (b) 6 wt% and (c) 12 wt% of uncoated nanoparticles. Here numbers 1 through 3 denote sample number.

5.2 Breakdown strength and pre-breakdown currents

Results from the breakdown strength and the pre-breakdown currents study were discussed in Papers V - VIII. These results can be summarized as follows:

1. Particle size: There seems to be no influence of the particle size on the measured breakdown strength in dry conditions (with exception for materials filled with amino-treated nanoparticles). For the wet case, however, the breakdown strength reduces more for the materials filled with the smaller (NA) nanoparticles in comparison to the ones filled with the bigger (ND) nanoparticles, see

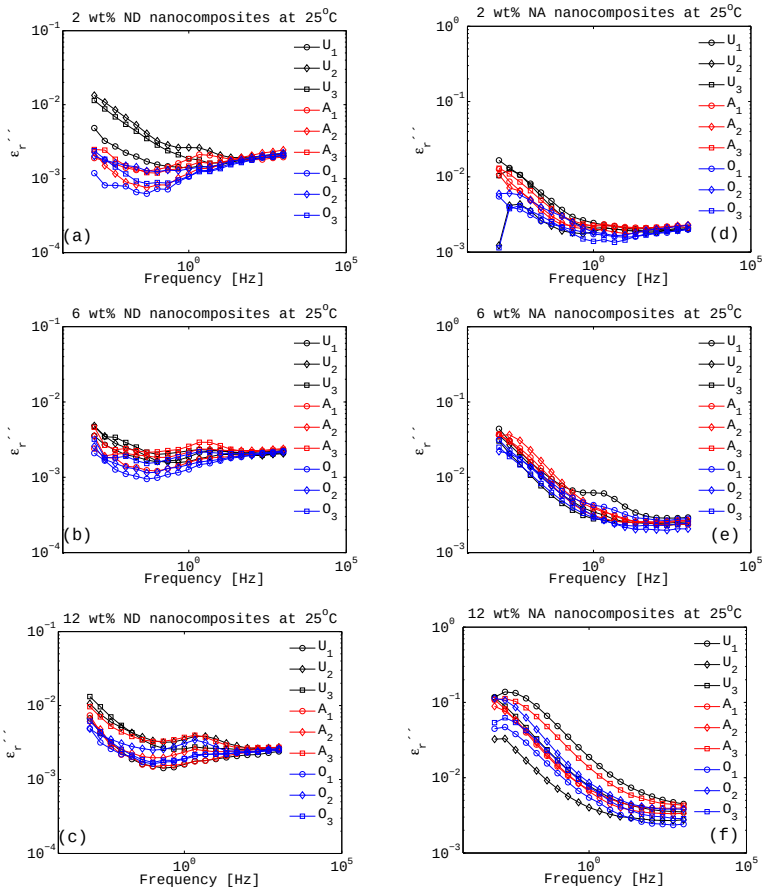

Figure 5.2: Influence of nanoparticle surface-modification on the dielectric loss as a function of frequency for the dry materials filled with (a) 2 wt%, (b) 6 wt%, (c) 12 wt% of ND nanoparticles and (d) 2 wt%, (e) 6 wt%, (f) 12 wt% of NA nanoparticles. Here numbers 1 through 3 stand for the number of the sample in the dry study.

Table 3 in Paper VI. Regarding the pre-breakdown currents it can be seen that the spread in the measured data is higher for the smaller (NA) nanoparticles in comparison to the larger (ND) nanoparticles in the dry conditions, see Fig. 8 in Paper VII, likely due to the higher sensitivity to moisture for the materials filled with NA nanoparticles. It can also be pointed out that the increase in the pre-breakdown current at high electric fields for the smaller nanoparticles seems to be steeper.

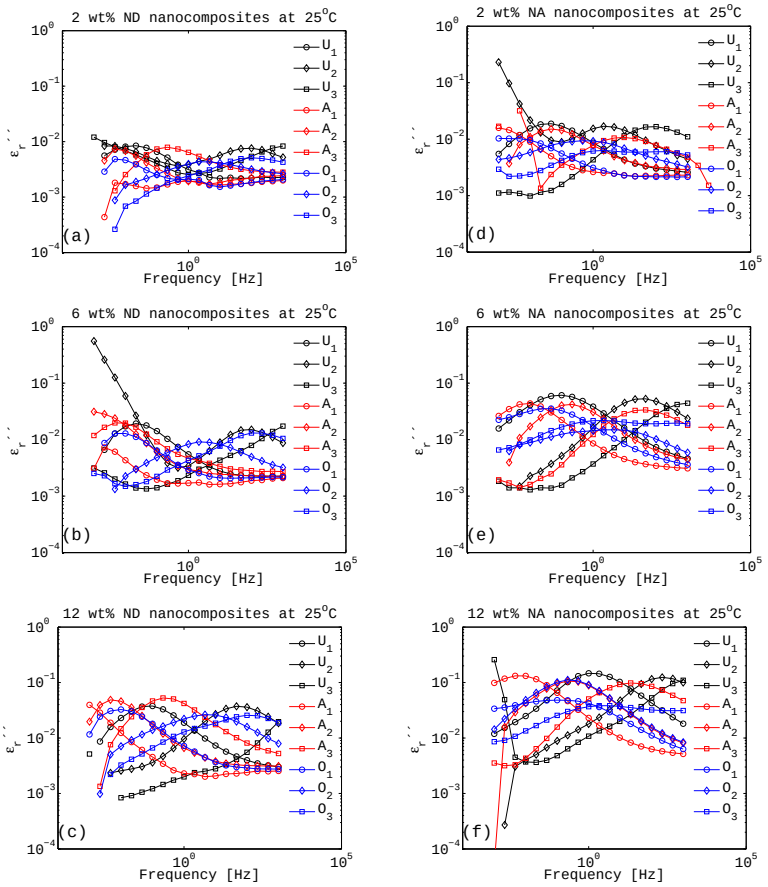

Figure 5.3: Influence of nanoparticle surface-modification on the dielectric loss as a function of frequency for the wet materials filled with (a) 2 wt%, (b) 6 wt%, (c) 12 wt% of ND nanoparticles and (d) 2 wt%, (e) 6 wt%, (f) 12 wt% of NA nanoparticles. Here numbers 1 through 3 stand for the type of humid conditioning, i.e. 1 corresponds to 24 %RH, 2 - 54 %RH and 3 - 86 %RH.

2. Nanoparticle surface modification type: The NDA6 can be pointed out as the most promising material formulation from the perspective of the highest breakdown strength among all the tested materials, which is clearly above 460 kV/mm in dry conditions, and the lowest pre-breakdown current for the tested nanocomposite materials. An attempt was made to estimate a value for the breakdown strength, see Appendix C for the details. The breakdown strength of the dry NDA6 nanocomposite was estimated to be in the interval between 500 and 755 kV/mm, likely in the lower part of the interval. In the wet con-

ditions the breakdown strength of the NDA6 is close to that of the reference unfilled material. There seems to be very little difference for the breakdown strength values for the materials filled with either uncoated or octyl-silanized nanoparticles. The same trend does not hold, however, for the materials filled with NA nanoparticles. For the pre-breakdown currents it can be seen that the influence of the surface modification is of more significance for the larger (ND) nanoparticles in comparison to the NA ones, see Fig. 11 in Paper VII. The currents for the materials filled with the uncoated nanoparticles are the largest in magnitude, followed by the currents for the materials filled with the octyl surface-treated nanoparticles and finally the currents corresponding to the amino surface modification. This trend is even more pronounced in wet conditions. For the smaller (NA) nanoparticles, however, this trend does not hold. It can be seen that in both dry and wet conditions the current for the materials filled with the untreated nanoparticles tends to be the largest of the three, but the magnitudes of the currents for the materials filled with surface-treated NA nanoparticles seem to be very similar.

3. Filler content: Only two samples per material filled with 2 and 12 wt% of octyl-silanized ND nanoparticles were tested in order to see if there is any trend in the data with respect to filler content. Comparing this data to the NDO6 in dry conditions points towards higher breakdown strength for the 6 wt% filler content, which could indicate that the optimal filler content lies close to 6 wt% filler content. While in wet conditions the breakdown strength reduces with increasing filler content, which follows the same trend as outlined in [28], [29].The pre-breakdown currents for all three filler contents in dry conditions seem to be very close in magnitude. In wet conditions, however, it can be seen that the current at high fields (above approximately 100 kV/mm) tends to increase with increasing filler content, see Fig. 10 in Paper VII.

4. Temperature: Temperature has a negative influence on the breakdown process, i.e. the time to breakdown reduces and the current through the tested materials increases with increasing temperature as shown in Paper VIII. The nanofilled materials are more stable than the reference unfilled material, as almost all the nanocomposite samples survive the testing when the reference unfilled material fails at temperatures above room temperature and under application of 22.5 kV_{DC}.

5. Humidity: In dry conditions the differences in the breakdown strength between the studied materials (with exception for NDA6) are very small, most are within the error margins as can be seen in Fig. 9 Paper VI. The breakdown strength of the nanocomposite materials is expected to reduce with increasing absorbed moisture content, see e.g. [30], [31], [29], [32], which corresponds well with the findings reported in Paper VI. For the reference unfilled materials with antioxidants the difference in the breakdown strength is within the error margin, see Fig. 9 in Paper VI. Pre-breakdown currents

tend to increase with increasing moisture absorption, see Fig. 9 in Paper VII. The spread in the measured data is smaller for the wet case and the threshold electric field at which the constant region stops decreases with increased moisture absorption.

5.3 On the importance of the total specific surface area for evaluation of the dielectric properties

Maximum *total specific surface area* (TSSA) is a theoretical maximum of surface area of nanoparticles in a nanocomposite available for creating an interaction zone. It can be said that generally the materials with larger TSSA are filled with the smaller nanoparticles (i.e. NA) and/or higher filler content. This area is highly reactive and for the larger TSSA the agglomeration level is higher, the antioxidants get adsorbed on the nanoparticles' surfaces to a larger extent and larger amount of water is absorbed by the nanocomposite material.

Naturally agglomeration causes a reduction in TSSA, but the agglomeration is not allowed to exceed a certain amount, for a material to be still considered a nanocomposite.

Adsorption of the antioxidants on the nanoparticles' surfaces is directly connected to OIT (oxidation induction time), which is a measure of how easy it is to oxidize a polymer. Higher adsorption of the antioxidants means that the effective amount of the antioxidants in a material reduces and, consequently, the OIT value reduces as well [57].

Higher water absorption points towards the possibility that the concentration of the hydroxyl groups available in the interfacial zone steers material properties of the nanocomposite materials. Higher water uptake results, for example, in lower breakdown strength and higher pre-breakdown currents. For the dielectric loss the higher water uptake means shifting of the loss peak towards higher frequencies in Arrhenius-like behavior.

In this work strong correlation was found between the OIT values and breakdown strength. We believe that the true reason behind this correlation is the connection between the water absorption and OIT values which both are a consequence of too high TSSA.

Surface treatment of the nanoparticles' surfaces can be understood as replacement of the hydroxyl groups with silane. If TSSA is larger than a certain threshold value then the influence of surface treatment on dielectric properties reduces.

These findings support the idea of optimal filler loading in a nanocomposite mate-

rial [16], which can be seen as the optimal TSSA, reflecting such factors as particle size, filler content, nanoparticle surface modification, degree of agglomeration and the reactivity of the silane used for the surface modification of the nanoparticles.

Chapter 6

Summary of publications

Paper I

In Paper I the dielectric permittivity of the dry nanocomposite materials and the reference unfilled material was presented as a function of frequency. The Havriliak-Negami approximation was used in order to justify the experimental data. For the unfilled material two relaxation peaks were suggested, unfortunately both of the loss peak frequencies were outside the measured frequency range. It was suggested that the loss peak corresponding to the higher frequency could be caused by polar butyl acrylate groups, while the loss peak at the lower frequency was a consequence of Maxwell-Wagner polarization. The dielectric losses for the nanocomposite materials are generally higher than for the reference unfilled material, but the differences in loss between different nanocomposites are small. The low frequency dispersion seemed to be affected by the addition of the nanoparticles.

Paper II

The influence of moisture absorption on the dielectric permittivity and $\tan\delta$ of the nanocomposite materials and the reference unfilled material was presented in Paper II. The data was analyzed with respect to the type of the nanoparticles surface modification, filler content and the level of humidity used for sample conditioning. It was found that the surface functionalization had a significant influence on the dielectric losses - both the magnitude of $\tan\delta$ and the frequency dependence. It was suggested that the absorbed water could bind to the remaining hydroxyl groups on the nanoparticles surfaces and also react with the silane used for surface treatment. It was shown that the magnitude of the loss peak was directly correlated to the filler content. As for the influence of the humidity level used for sample conditioning it was seen that the behavior of the dielectric loss peaks resembles Arrhenius activation when the loss peaks are shifted towards higher frequencies with the increased humidity level.

Paper III

In Paper III the dielectric permittivity and $\tan\delta$ were evaluated for the dry nanocomposite materials studied in this work along with the unfilled reference material. The analysis was performed with respect to particle size, type of surface modification used, temperature and filler content. It was found that only materials filled with the smaller (NA) nanoparticles exhibited loss peaks, while the low frequency dispersion was characteristic of the materials filled with the bigger (ND) nanoparticles. The surface modification did not seem to have a pronounced effect on the resulting $\tan\delta$ for the dry nanocomposites. As for the influence of temperature Arrhenius activation was observed and the activation energies were estimated for every studied material.

Paper IV

Paper IV was written in conjunction with the Paper III. Here the data for the dielectric permittivity and $\tan\delta$ was presented for the nanocomposite materials and unfilled reference material after conditioning at a given humidity level. The analysis was performed with respect to particle size, surface modification, filler content and humidity. Dielectric loss measured for the unfilled reference material indicated that the loss peak increased in magnitude with increasing water absorption while keeping the same frequency dependence, which implied that any changes in frequency dependence of the dielectric losses of the nanocomposite materials would arise due to the presence of the nanoparticles. It was shown that the dielectric losses increased with decreasing size of the nanofiller. The influence of nanoparticles' surface treatment on the dielectric loss of the nanocomposite materials was profound. Increasing filler content caused increasing dielectric losses with a slight shift towards higher frequencies. The increasing moisture absorption caused a very distinct shift in frequency behavior of $\tan\delta$ loss peak towards higher frequencies with almost no changes in the magnitude.

Paper V

Dielectric breakdown strength of the nanocomposite materials filled with NanoDur alumina nanoparticles along with the unfilled reference material was evaluated in Paper V. This study was performed on both dry materials and after conditioning in air with 86 %RH. Weibull statistics was applied to the measured data. As expected water absorption caused a reduction of the breakdown strength. It was shown that surface treatment of the nanoparticles with amino silane had a positive influence on the breakdown strength. In fact the nanocomposite filled with the amino-treated nanoparticles had highest breakdown strength in dry conditions and almost the same breakdown strength as the unfilled reference material after conditioning in humid environment. The rest of the nanocomposite materials in dry conditions had similar values of breakdown strength to the reference unfilled material with

considerable reduction in breakdown strength with absorbed moisture. It was also found that breakdown strength data for the nanocomposite materials was more predictable than for the unfilled reference material.

Paper VI

Paper VI is a supplemented and enlarged continuation of Paper V. Here the breakdown strength data for the nanocomposite materials filled with either NanoDur or NanoAmor along with the data for the unfilled reference material is presented. As in Paper V the study was performed both in dry conditions and after conditioning in a humid environment at 86 %RH. It is argued that the effective specific surface area is a very important factor influencing breakdown strength and the analysis is performed with the latter parameter in mind rather than particle size and filler content. The influence of water absorption on the breakdown strength is illustrated.

Paper VII

Paper VII was written in conjunction with Paper VI and presents the measured pre-breakdown currents during breakdown strength testing. The data is analyzed according to space-charge limited conduction theory and threshold values between different conduction regimes are obtained. It can be seen that conditioning in humid environment causes the increase in the pre-breakdown current. It is also shown that there is an inverse proportionality between the extracted threshold field strengths and the effective specific surface area.

Paper VIII

Paper VIII presents the results obtained from a constant stress testing study performed at temperatures above room temperature. The findings in this paper show that the nanocomposite materials are more stable with respect to temperature, i.e. most of the nanofilled materials survive testing at temperatures above room temperature while the reference unfilled materials do not. It was also shown that the time to breakdown reduces and the current through a material increases with increasing temperature. Surface treatment of the nanoparticles with amino-silane prior to dispersing in the host polymer matrix has a positive impact on the materials properties, i.e. the current through the material is smaller for the nanocomposites filled with surface-treated nanoparticles.

Chapter 7

Conclusions and future work

7.1 Conclusions

The electric properties of the poly(ethylene-*co*-butyl acrylate) filled with alumina nanoparticles with varying filler content, surface modification and particle type were studied in this work. The chosen properties were dielectric permittivity and losses as well as breakdown strength and the pre-breakdown currents.

The dielectric permittivity and losses were analyzed with the following parameters in mind: particle size, filler content, surface modification of the nanoparticles, temperature and humidity. It was found that the particle size had a distinct influence on the dielectric losses with higher losses for the smaller nanoparticles. The increasing filler content was shown to cause the increase in the dielectric loss. It was seen that the surface modification of the nanoparticles had almost no influence on the dielectric loss if the tested materials were thoroughly dried. For the samples conditioned in humid environment on the other hand surface modification of the nanoparticles prior to dispersing the latter in the host matrix played a significant role. The influence of temperature on the dielectric loss can be accounted by Arrhenius activation behavior. It was shown that the amount of absorbed moisture determined the frequency behavior of the dielectric losses.

Analyzing data from the breakdown strength study suggested the existence of optimal total specific surface area, which reflects such factors as particle size, filler content, nanoparticle surface modification, degree of agglomeration and the reactivity of the silane used for the surface modification of the nanoparticles. This supports the idea of optimal filler loading in a nanocomposite material.

Studying the pre-breakdown currents it was concluded that the space-charge limited conduction is likely and the transitions between the different conduction regimes could be used as indication of the material stability.

In my opinion one of the most important results in this study was the illustration of the impact of absorbed moisture on the electric insulating properties of the nanocomposite materials.

7.2 Future work

There are a number of possible ideas that could be further developed as a continuation of this project. Here I am going to mention a few:

1. Perform electrical treeing experiments, which should result in longer inception and propagation times for the nanocomposite materials in comparison to the unfilled reference material. This is expected due to a good dispersion of the nanoparticles in the host matrix.

2. Confirm the space-charge limited conduction mechanism by using several different thicknesses of the samples as the current density is inversely proportional to the sample thickness, see Eq.(7.1) [47]

$$J = \frac{9}{8}\epsilon_0\epsilon_r\mu\frac{V^2}{L^3} \tag{7.1}$$

3. Measure space charge up to breakdown, which could help in estimating trapping energy levels for the materials in question. A reduced space charge is expected for the nanocomposites in comparison to the unfilled host material.

4. Measure breakdown strength with polarity reversal. The values are expected to be higher for the nanocomposite materials in comparison to the unfilled host material due to the lower space charge.

5. Perform an electroluminescence study.

6. Compare the dielectric properties of the nanocomposite materials to those of the microfilled materials.

7. Create a mathematical model to explain the dielectric properties of the nanocomposite materials.

8. Evaluate influence of electrode surface roughness on the breakdown strength and pre-breakdown current.

Appendix A

A: Dielectric spectroscopy - dry case

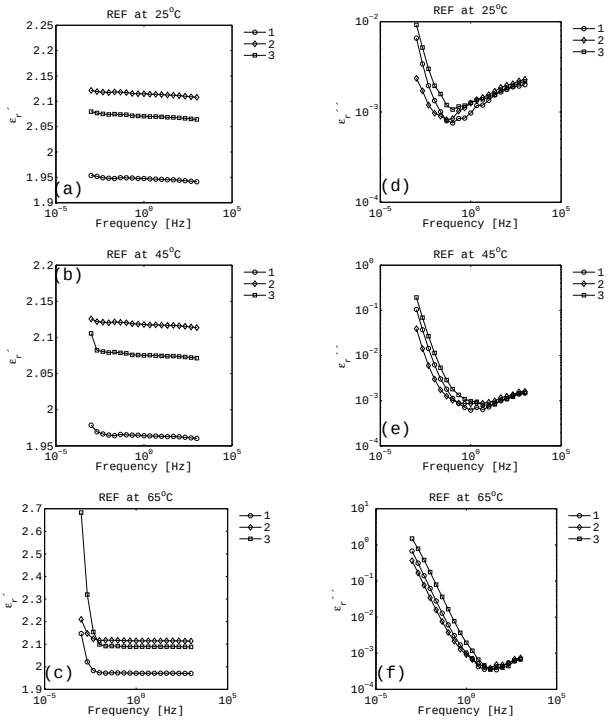

Figure A.1: (a-c) Relative dielectric constant and (d-f) corresponding dielectric loss as a function of frequency measured for the reference unfilled material at (a, d) 25 $°C$, (b, c) 45 $°C$ and (c, f) 65 $°C$. Here numbers 1 through 3 denote different samples.

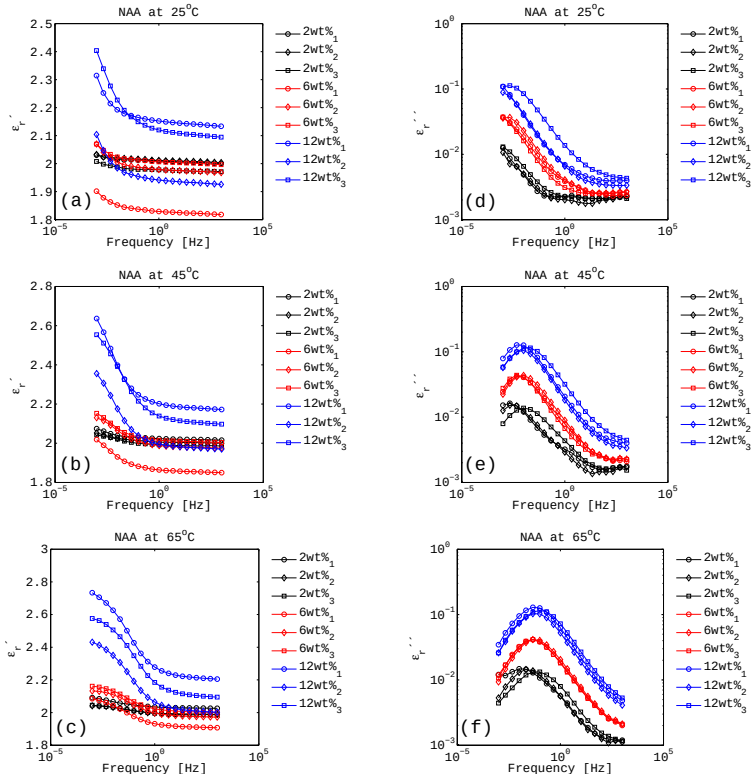

Figure A.2: (a-c) Relative dielectric constant and (d-f) corresponding dielectric loss as a function of frequency for varying filler content measured for the poly(ethylene-*co*-butyl acrylate) filled with amino-treated NA nanoparticles at (a, d) 25 $^{\circ}C$, (b, c) 45 $^{\circ}C$ and (c, f) 65 $^{\circ}C$. Here numbers 1 through 3 denote different samples.

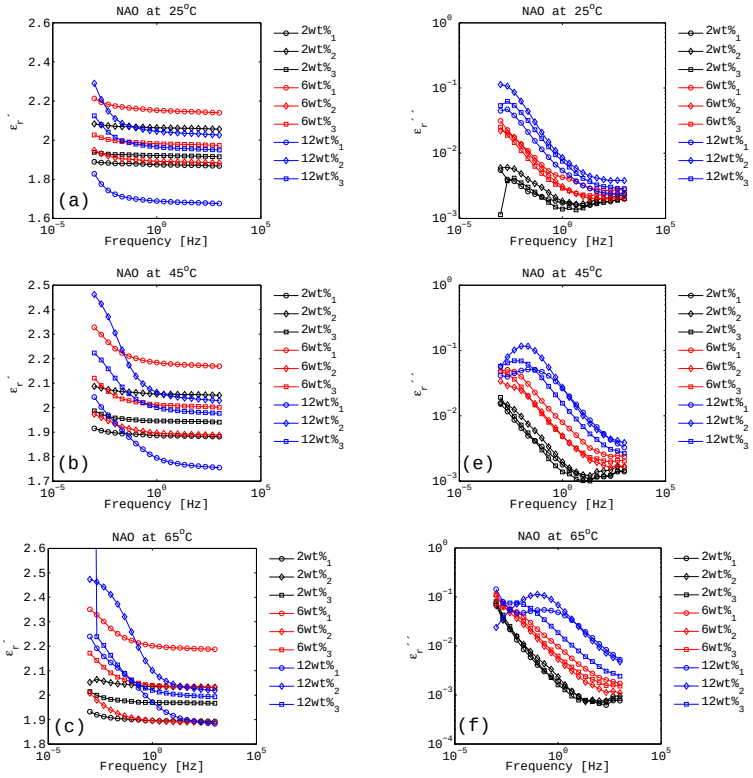

Figure A.3: (a-c) Relative dielectric constant and (d-f) corresponding dielectric loss as a function of frequency for varying filler content measured for the poly(ethylene-*co*-butyl acrylate) filled with octyl-treated NA nanoparticles at (a, d) 25 $^{\circ}C$, (b, c) 45 $^{\circ}C$ and (c, f) 65 $^{\circ}C$. Here numbers 1 through 3 denote different samples.

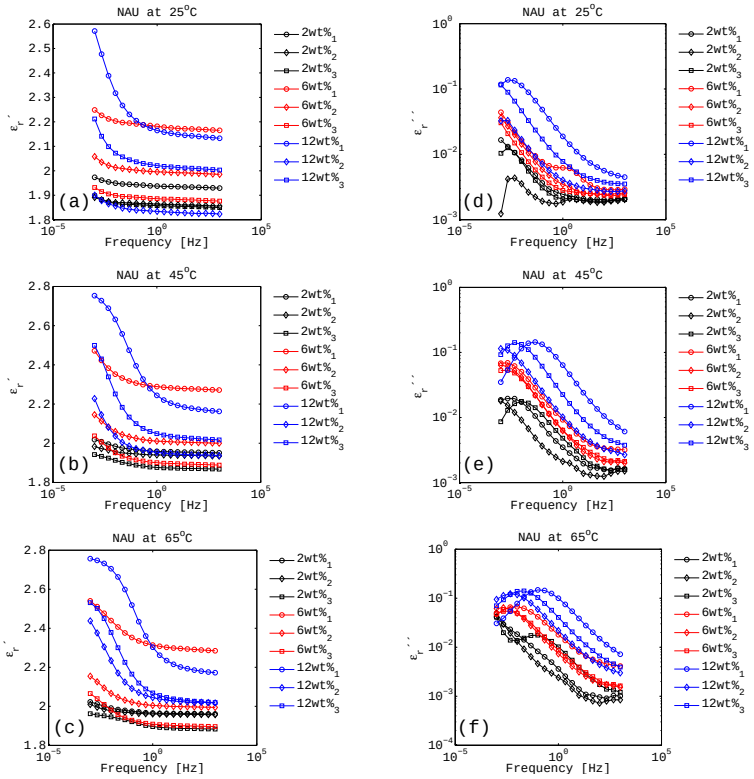

Figure A.4: (a-c) Relative dielectric constant and (d-f) corresponding dielectric loss as a function of frequency for varying filler content measured for the poly(ethylene-*co*-butyl acrylate) filled with untreated NA nanoparticles at (a, d) 25 $^{\circ}C$, (b, c) 45 $^{\circ}C$ and (c, f) 65 $^{\circ}C$. Here numbers 1 through 3 denote different samples.

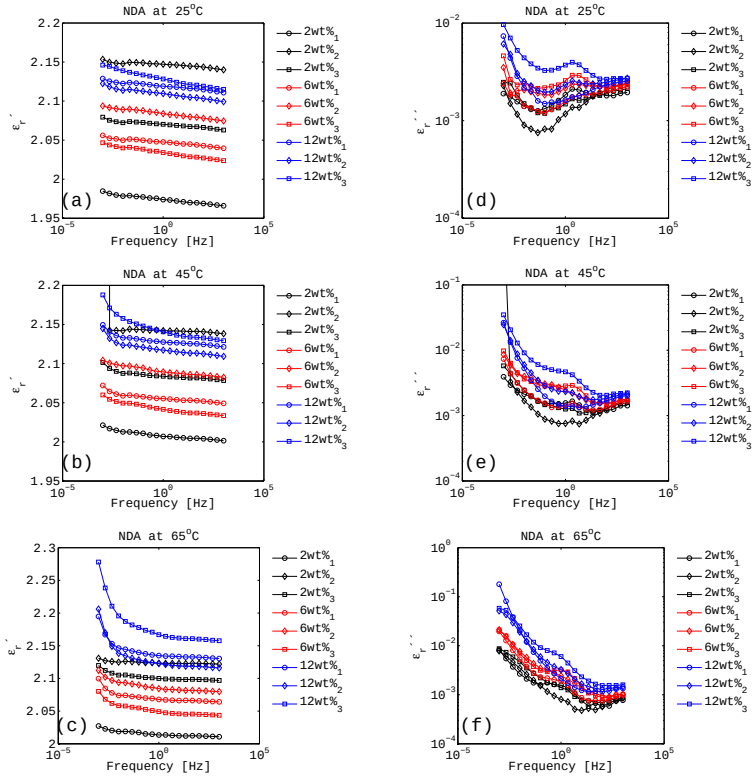

Figure A.5: (a-c) Relative dielectric constant and (d-f) corresponding dielectric loss as a function of frequency for varying filler content measured for the poly(ethylene-*co*-butyl acrylate) filled with amino-treated ND nanoparticles at (a, d) 25 $°C$, (b, c) 45 $°C$ and (c, f) 65 $°C$. Here numbers 1 through 3 denote different samples.

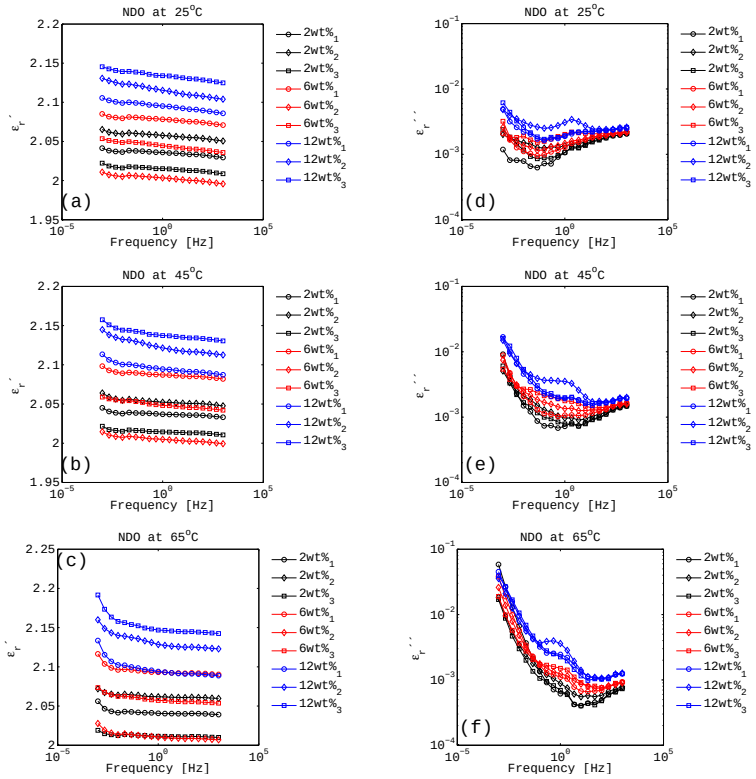

Figure A.6: (a-c) Relative dielectric constant and (d-f) corresponding dielectric loss as a function of frequency for varying filler content measured for the poly(ethylene-*co*-butyl acrylate) filled with octyl-treated ND nanoparticles at (a, d) 25 $^{\circ}C$, (b, c) 45 $^{\circ}C$ and (c, f) 65 $^{\circ}C$. Here numbers 1 through 3 denote different samples.

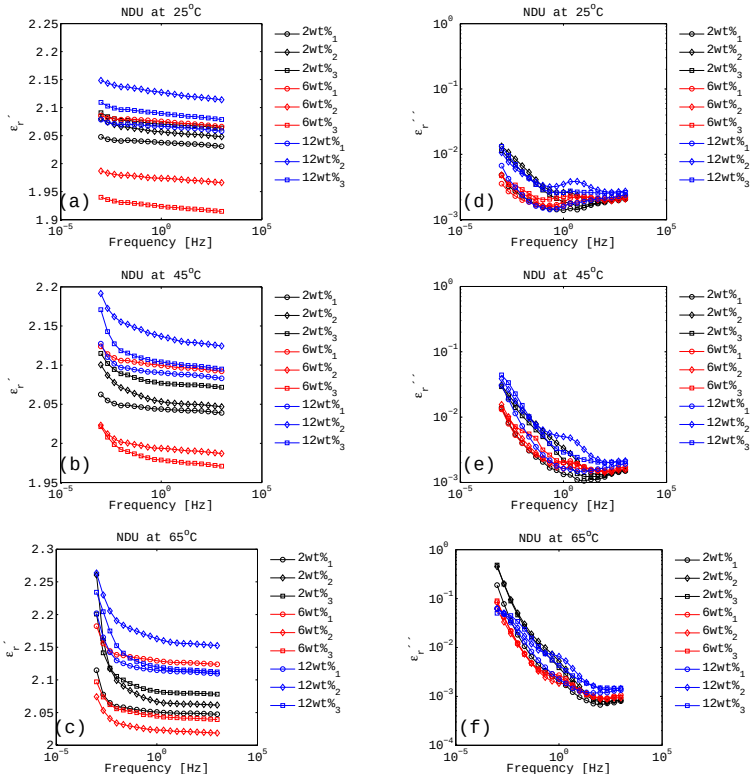

Figure A.7: (a-c) Relative dielectric constant and (d-f) corresponding dielectric loss as a function of frequency for varying filler content measured for the poly(ethylene-*co*-butyl acrylate) filled with untreated ND nanoparticles at (a, d) 25 $^{\circ}C$, (b, c) 45 $^{\circ}C$ and (c, f) 65 $^{\circ}C$. Here numbers 1 through 3 denote different samples.

Appendix B

B: Dielectric spectroscopy - wet case

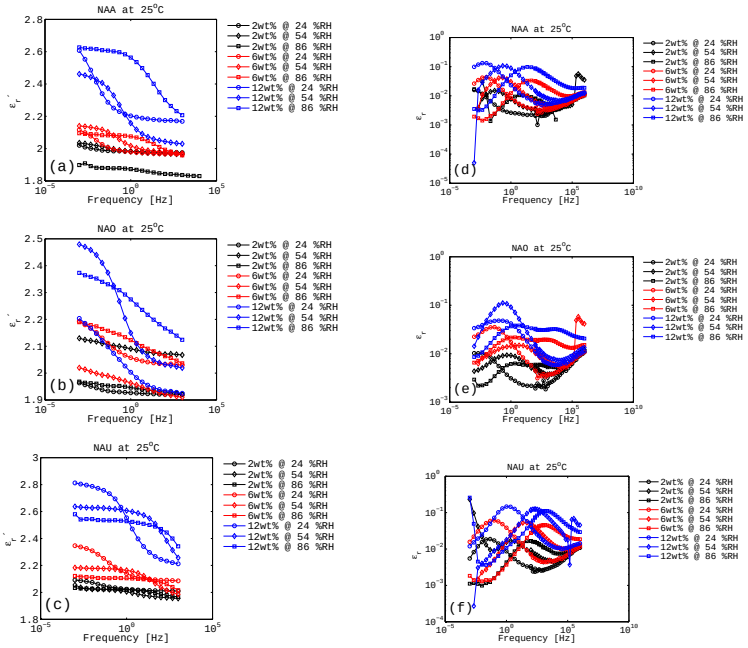

Figure B.1: (a-c) Relative dielectric constant and (d-f) corresponding dielectric loss as a function of frequency for varying filler and moisture content measured for the poly(ethylene-*co*-butyl acrylate) filled with (a, d) amino-treated, (b, c) octyl-treated and (c, f) untreated NA nanoparticles.

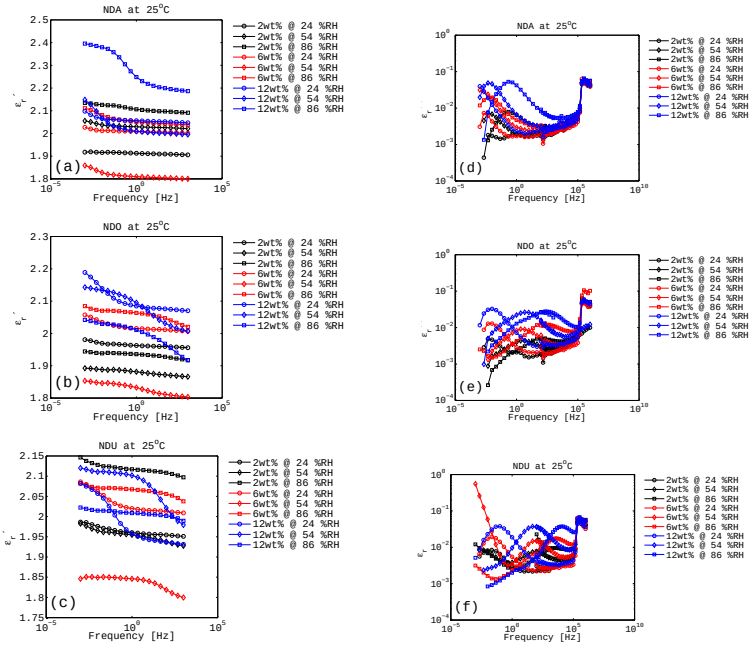

Figure B.2: (a-c) Relative dielectric constant and (d-f) corresponding dielectric loss as a function of frequency for varying filler and moisture content measured for the poly(ethylene-*co*-butyl acrylate) filled with (a, d) amino-treated, (b, c) octyl-treated and (c, f) untreated ND nanoparticles.

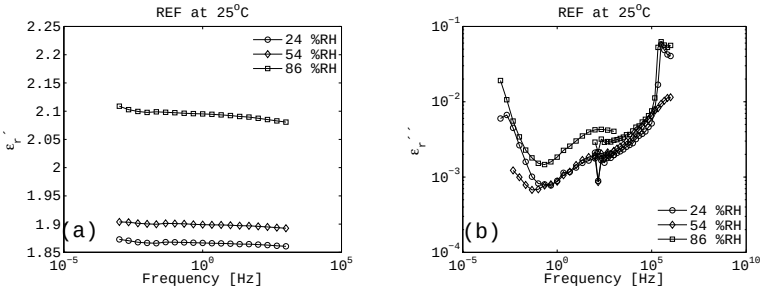

Figure B.3: (a) Relative dielectric constant and (b) corresponding dielectric loss as a function of frequency for varying moisture content measured for the unfilled reference material

Appendix C

C: Estimate of α for the dry NDA6

It is hard to give a good estimate of the 63% probability failure for the dry NDA6 composite, i.e. α, as only three samples out of ten broke down. This material formulation is the most interesting one in the experimental matrix due to highest breakdown strength. The first strategy is simply to apply the Weibull distribution on the three available points. Following the strategy outlined in [58], the following table was constructed, see Table C.1. All the notations used here were explained in [58] and Paper VI. In Fig. C.1 the $ln(-ln(1-F(i,n))/100)$ is plotted versus breakdown strength values both for the experimentally obtained data as well as the rough approximation based on 3 experimental points. Finding the intersection between the line corresponding to the 63% probability of breakdown and the approximated line, it is possible to estimate α parameter to be approximately 500 kV/mm. This estimation is rough. In order to obtain a more accurate value a larger sample size is needed for obtaining good statistical justification. Knowing that the thickness of the NDA6 samples is approximately 130 μm, implies that breakdown strength of 500 kV/mm would demand a voltage source capable of creating a controlled DC voltage ramp up to at least 65 kV. Higher voltage cap would be preferable in order to ascertain reaching the breakdown as the analysis indicating α equal to 500 kV/mm is rough. This in turn demands testing at least two materials, one of which should be well described (e.g. dry NDU6) in order to compare the experimental setups and the second one would have to be dry NDA6.

Another approach for the estimation could be assuming that the measured

Table C.1: Calculating Weibull distribution data

Rank, i	E_i, [kV/mm]	$F(i,n) = (i-0.44)/(n+0.25) \cdot 100$ [%]	$ln(-ln\frac{1-F(i,n)}{100})$
1	397	5.5	-2.87
2	443	15.2	-1.80
3	450	25	-1.25

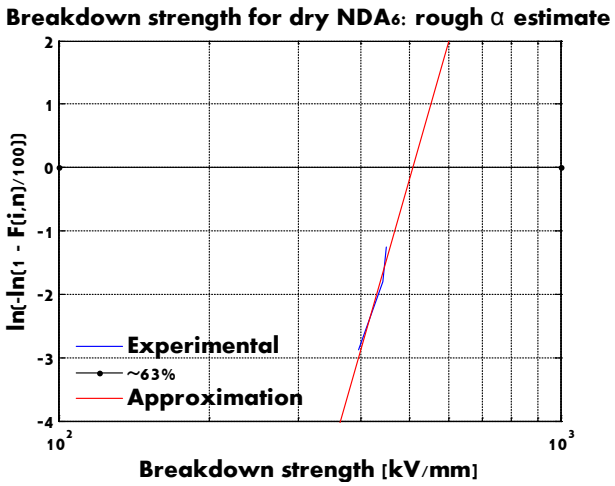

Figure C.1: Rough estimate of the α parameter for the dry NDA6

breakdown strengths for NDA6, namely 397, 443, and 450 kV/mm measured for the failed samples, can be thought off as the lowest three points in the Weibull distribution. Normalizing the three lowest breakdown strength values for NDU6 and NDO6 with the corresponding maximal breakdown strength, and comparing them, gives the estimate for the normalized values for the NDA6, see Table C.2. Multiplying the latter with the maximal breakdown strength for the dry NDA6 should produce the known lowest breakdown strengths. Averaging the obtained lowest breakdown strengths, gives 755 kV/mm. This value provides the maximum for the interval where the estimated value of the breakdown strength should fall into. So that the breakdown strength of the NDA6 nanocomposite can be estimated to be in the interval between 500 and 755 kV/mm, likely in the lower part of the interval.

Table C.2: Estimating breakdown strength of NDA6 based on the measured data for NDU6 and NDO6

Material	α_{dry} [kV/mm]	BDS_{max} [kV/mm]	α_{norm}	BDS_{norm}, for the 3 lowest points	Std(BDS_{norm}), for the 3 lowest points	Lowest breakdown strengths, [kV/mm]
REF	375	425	0.88			
NDU6	362	446	0.81	0.49, 0.63, 0.67		
NDA6	444	450	0.81, based on NDU6 and NDO6	0.47, 0.60, 0.66 based on NDU6 and NDO6	0.03, 0.05, 0.02, based on NDU6 and NDO6	845, 738, 683
NDO6	378	469	0.81	0.45, 0.57, 0.65		

Bibliography

[1] T.J. Lewis. Nanometric dielectrics. *IEEE Transactions on Dielectrics and Electrical Insulation*, 5:812 – 825, 1994.

[2] H.D. Alamdari M.F. Fréchette, M. Trudeau and S. Boily. Introductory remarks on nanodielectrics. In *Conference on Electrical Insulation and Dielectric Phenomena*, pages 92 – 99, 2001.

[3] N. Jäverberg. *Dielectric properties of poly(ethylene-co-butyl acrylate) filled with alumina nanoparticles*. Licentiate thesis, School of Electrical Engineering, 2011. Royal Institute of Technology (KTH).

[4] Y. Ohki Z. Li, K. Okamoto and T. Tanaka. The role of nano and micro particles on partial discharge and breakdown strength in epoxy composites. *IEEE Transactions on Dielectrics and Electrical Insulation*, 18(3):675 – 681, 2011.

[5] A. Krivda L.E. Schmidt D. Fabiani, G.C. Montanari and R. Hollertz. Epoxy based materials containing micro and nano sized fillers for improved electrical characteristics. In *10th IEEE International Conference on Solid Dielectrics*, pages 1 – 4, 2010.

[6] F. Palmieri V.H.A. Camara D. Fabiani, G.C. Montanari and A. Krivda. The effect of temperature on space charge behavior of epoxy resins containing both micro and nano sized fillers. In *Conference on Electrical Insulation and Dielectric Phenomena*, pages 648 – 651, 2011.

[7] Y. Ohki Z. Li, K. Okamoto and T. Tanaka. Effects of nano-filler addition on partial discharge resistance and dielectric breakdown strength of micro-Al_2O_3/epoxy composite. *IEEE Transactions on Dielectrics and Electrical Insulation*, 17(3):653 – 661, 2010.

[8] M. Nagao Y. Sekiguchi Ch. C. Reddy S. Okuzumi, Y. Murakami and Y. Murata. DC breakdown strength and conduction current of MgO/LDPE composite influenced by filler size. In *Annual Report Conference on Electrical Insulation Dielectric Phenomena*, pages 722 – 725, 2008.

[9] T.J. Lewis. Interfaces are the dominant feature of dielectrics at the nanometric level. *IEEE Transactions on Dielectrics and Electrical Insulation*, 11(5):739 – 753, 2004.

[10] R.K. MacCrone L.S. Schadler C.W. Reed M. Roy, J.K. Nelson and R. Keefe. Polymer nanocomposite dielectrics - the role of the interface. *IEEE Transactions on Dielectrics and Electrical Insulation*, 12(4):629 – 643, 2005.

[11] R. W. Siegel. What do we really know about the atomic-scale structures of nanophase materials? *Journal of Physics and Chemistry of Solids*, 55(10):1097 – 1106, 1994.

[12] P. Nordell S. Nawaz B. Azhdar N. Jäverberg, H. Edin and U.W. Gedde. Dielectric properties of alumina-filled poly(ethylene-*co*-butyl acrylate) nanocomposites, part i - dry studies. *IEEE Transactions on Dielectrics and Electrical Insulation*, 19(2):383 – 390, 2012.

[13] P. Nordell S. Nawaz B. Azhdar N. Jäverberg, H. Edin and U.W. Gedde. Dielectric properties of alumina-filled poly(ethylene-*co*-butyl acrylate) nanocomposites, part ii - wet studies. *IEEE Transactions on Dielectrics and Electrical Insulation*, 19(2):391 – 399, 2012.

[14] T. Tanaka. Dielectric nanocomposites with insulating properties. *IEEE Transactions on Dielectrics and Electrical Insulation*, 12(5):914 – 928, 2005.

[15] By an international collective of scientists. Nanodielectrics: a panacea for solving all electrical insulation problems? In *International Conference on Solid Dielectrics*, pages 1 – 29, 2010.

[16] M. Takala. *Electrical insulation materials towards nanodielectrics*. Doctoral thesis, 2010. Tampere university of technology.

[17] Y.Y. Huang and E.M. Terentjev. Tailoring of electrical properties of carbon nanotube-polymer composites. *Advanced Functional Materials*, 20:4062 – 4068, 2010.

[18] P.S. Casey R.J. Flemming, A. Ammala and S.B. Lang. Conductivity and space charge in LDPE containing nano- and micro-sized ZnO particles. *IEEE Transactions on Dielectrics and Electrical Insulation*, 15(1):118 – 126, 2008.

[19] A. Sihvola. *Electromagnetic Mixing Formulas and Applications*. The Institution of Electrical Engineers, 1999.

[20] Z. Hu X. Huang, L. Xie and P. Jiang. Influence of $BaTiO_3$ nanoparticles on dielectric, thermophysical and mechanical properties of ethylene-vinyl acetate elastomer/$BaTiO_3$ microcomposites. *IEEE Transactions on Dielectrics and Electrical Insulation*, 18(2):375 – 383, 2011.

[21] T. Marinis Y. Rao, J. Qu and C.P. Wong. A precise numerical prediction of effective dielectric constant for polymer-ceramic composite based on effective-medium theory. *IEEE Transactions on Components and Packaging Technologies*, 23(4):680 – 683, 2000.

[22] R.E. DuBroff M.Y. Koledintseva and R.W. Schwartz. A maxwell garnett model for dielectric mixtures containing conducting particles at optical frequencies. *Progress in Electromagnetics Research*, 63:223 – 242, 2006.

[23] T. Tanaka. Nanodielectrics: how does the presence of interfaces influence behavior? In *International Conference on Power and Energy Systems*, pages 1 – 4, 2011.

[24] M. Fréchette J. Castellon D. Fabiani G.C. Montanari R. Gorur P. Morshuis S. Gubanski J. Kindersberger A. Vaughn S. Pelissou Y. Tanaka L.E. Schmidt G. Iyer T. Andritsch J. Seiler A. Krivda, T. Tanaka and M. Anglhuber. Characterization of epoxy microcomposite and nanocomposite materials for power engineering applications. *IEEE Insulation Magazine*, 28(2):38 – 51, 2012.

[25] G.C. Montanari Y. Tanaka Y. Ohki A. Bulinski S. Gubanski M. Nagao S. Pélissou C.W. Reed J. Castellon J. Kindersberger P. Morshuis A. Vaughan S. Sutton T. Tanaka, M. Fréchette and S.J. Han. Dielectric properties of XLPE/SiO_2 nanocomposites based on CIGRE WG D1.24 cooperative test results. *IEEE Transactions on Dielectrics and Electrical Insulation*, 18(5):1484 – 1517, 2011.

[26] R. Richert A. Krivda G. Iyer, R.S. Gorur and L.E. Schmidt. Dielectric properties of epoxy based nanocomposites for high voltage insulation. *IEEE Transactions on Dielectrics and Electrical Insulation*, 18(3):659 – 666, 2011.

[27] P. Nevalainen P. Pakonen J. Pelto M. Karttunen S. Virtanen V. Koivu M. Pettersson B. Sonerud M. Takala, H. Ranta and K. Kannus. Dielectric properties and partial discharge endurance of polypropylene-silica nanocomposite. *IEEE Transactions on Dielectrics and Electrical Insulation*, 17(4):1259 – 1267, 2010.

[28] P. Morshuis T. Andritsch, R. Kochetov and J.J. Smit. Short term DC breakdown and complex permittivity of Al_2O_3- and MgO-epoxy nanocomposites. In *Annual Report Conference on Electrical Insulation and Dielectric Phenomena*, pages 1 – 4, 2010.

[29] M. Reading and A.S. Vaughan. Rheological, thermal and electrical properties of poly(ethylene oxide)/boehmite nanocomposites. In *Annual Report Conference on Electrical Insulation and Dielectric Phenomena*, pages 576 – 579, 2009.

[30] J.K. Nelson L. Hui and L.S. Schadler. The influence of moisture on the electrical performance of XLPE/silica nanocomposites. In *International Conference on Solid Dielectrics*, pages 1 – 4, 2010.

[31] J.K. Nelson L. Hui and L.S. Schadler. Hydrothermal aging of XLPE/silica nanocomposites. In *Annual Report Conference on Electrical Insulation and Dielectric Phenomena*, pages 1 – 4, 2010.

[32] G.C. Montanari D. Fabiani and L. Testa. Effect of aspect ratio and water contamination on the electric properties of nanostructured insulating materials. *IEEE Transactions on Dielectrics and Electrical Insulation*, 17(1):221 – 230, 2010.

[33] M. Nagao M. Ieda and M. Hikita. High-field conduction and breakdown in insulating polymers. *IEEE Transactions on Dielectrics and Electrical Insulation*, 1(5):934 – 945, 1994.

[34] U. Lafont P. Morshuis R. Kochetov, T. Andritsch and J.J. Smit. Effects of inorganic nanofillers and combinations of them on the complex permittivity of epoxy-based composites. In *IEEE International Symposium on Electrical Insulation*, pages 1 – 5, 2010.

[35] S. Agnel A. Toureille M. Fréchette S. Savoie A. Krivda J. Castellon, H.N. Nguyen and L.E. Schmidt. Electrical properties analysis of micro and nano composite epoxy resin materials. *IEEE Transactions on Dielectrics and Electrical Insulation*, 18(3):651 – 658, 2011.

[36] Y. Ohki T. Tanaka Y. Sekiguchi Y. Murata K. Ishimoto, E. Kanegae and C.C. Reddy. Superiority of dielectric properties of LDPE/MgO nanocomposites over microcomposites. *IEEE Transactions on Dielectrics and Electrical Insulation*, 16(6):1735 – 1742, 2009.

[37] E. David A. Sami, M.F. Fréchette and S. Savoie. Water as a digression relative to the dielectric response in the frequency domain for polymer composites. In *Annual Report Conference on Electrical Insulation and Dielectric Phenomena*, pages 501 – 504, 2008.

[38] J.C. Fothergill C. Zou and S.W. Rowe. The effect of water absorption on the dielectric properties of epoxy nanocomposites. *IEEE Transactions on Dielectrics and Electrical Insulation*, 15(1):106 – 117, 2008.

[39] A.K. Jonscher. *Dielectric relaxation in solids*. Chelsea Dielectrics Press, 1983. ISBN: 0-95087-110-9.

[40] S. Basu V. Parameswaran P. Maity, P.K. Poovamma and N. Gupta. Dielectric spectroscopy of epoxy resin with and without nanometric alumina fillers. *IEEE Transactions on Dielectrics and Electrical Insulation*, 16(5):1481 – 1488, 2009.

[41] International Standard IEC 60243-1. *Electrical strength of insulating materials - test methods*, 1998. 2nd ed.

[42] P. Nordell. *Aluminium oxide - poly(ethylene-co-butyl acrylate) nanocomposites: synthesis, structure, transport properties and long-term performance.* Licentiate thesis, Fibre and Polymer Technology, 2011. Royal Institute of Technology (KTH).

[43] J. D. Jackson. *Classical Electrodynamics.* John Wiley & Sons, Inc., New York, 1998. ISBN: 0-471-30932-X.

[44] D. K. Cheng. *Field and Wave Electromagnetics.* Addison Wesley, 1989. ISBN: 0-201-12819-5.

[45] R.K. Wangsness. *Electromagnetic Fields.* John Wiley & Sons, Inc., New York, 1986. ISBN: 0-471-81186-6.

[46] J.J. O'Dwyer. *The theory of electrical conduction and breakdown in solid dielectrics.* Clarendon Press, Oxford, 1973. ISBN: 0-19-851332-1.

[47] P. Mark M.A. Lampert. *Current injection in solids.* Academic press, New York, 1970. ISBN: 99915-57-33-4.

[48] J.C. Fothergill L.A. Dissado. *Electrical degradation and breakdown in polymers.* Peter Peregrinus Ltd., 1992. ISBN: 0-86341-196-7.

[49] C. Kittel. *Introduction to solid state physics.* John Wiley & Sons, Inc., New York, 1996. ISBN: 0-471-11181-3.

[50] E.J. McMahon R. Bartnikas, editor. *Engineering Dielectrics: Vol. IIA Electrical properties of solid insulating materials: molecular structure and electrical behavior.* American Society for Testing and Materials, 1983. ISBN: 99-0381000-8.

[51] W.S. Zaengl E. Kuffel and J. Kuffel. *High voltage engineering: fundamentals.* Newnes Press, Norfolk, 2005. ISBN: 0-7506-3634-3.

[52] Megger. Insulation diagnostic analyzer idax300. Available at: `http://www.megger.com/eu/products/ProductDetails.php?ID=1019&Description=IDAX300`.

[53] Agilent. Agilent 33120a 15 mhz function / arbitrary waveform generator: User's guide. Available at: `http://mntl.illinois.edu/equipment/docs/agilent33120auserguide.pdf`.

[54] Inc. Trek. High voltage power amplifier trek model 30 / 20a: Specification. Available at: `http://www.trekinc.com/pdf/30-20A_Sales.PDF`.

[55] Keithley. Instruction manual for model 427 current amplifier. Available at: `http://www-physics.ucsd.edu/neurophysics/courses/physics_173_273/Ithaco_Model_427_current_amplifier.pdf`.

[56] Tektronix. Tektronix tds3000 series digital phosphor oscilloscopes: User manual. Available at: `http://www.cs.washington.edu/education/courses/cse466/07wi/labs/l2/Oscope/TDS3000Manual.pdf`.

[57] S. Nawaz. *Preparation and long-term performance of poly(ethylene-co-butyl acrylate) nanocomposites and polyethylene*. Doctoral thesis, Fibre and Polymer Technology, 2012. Royal Institute of Technology (KTH).

[58] IEEE Std. 930 - 2004. *IEEE guide for the statistical analysis of electrical insulation breakdown data*, 2004.